Cement and Concrete Research 178 (2024) 107404

Contents lists available at ScienceDirect

Cement and Concrete Research

journal homepage: www.elsevier.com/locate/cemconres

Citrate sorption on cement hydrates

Rosa Ester Guidone [a,b,*], Xavier Gaona [b], Frank Winnefeld [a], Marcus Altmaier [b], Horst Geckeis [b], Barbara Lothenbach [a]

[a] Laboratory Concrete & Asphalt, Empa, Swiss Federal Laboratories for Materials Science and Technology, Überlandstrasse 129, 8600 Dübendorf, Switzerland
[b] Karlsruhe Institute of Technology (KIT), Institute for Nuclear Waste Disposal (INE), Hermann-von-Helmholtz-Platz 1, 76344 Eggenstein-Leopoldshafen, Germany

ARTICLE INFO

Keywords:
AFm phases
C-S-H
Sorption
Citrate

ABSTRACT

The interaction of citrate with hydrated Portland cement and its main hydrates: C-S-H ($0.8 \leq Ca/Si \leq 1.4$), ettringite, monosulfo-, hemi- and monocarboaluminate is investigated. The solubility of citrate-AFm and citrate-AFt was determined. Batch sorption experiments at pH = 13.2 showed that citrate sorbs relatively strongly on AFm phases and ettringite. Citrate sorbed only on the outer surfaces sites of monosulfoaluminate, monocarboaluminate and ettringite resulting in a low sorption capacity of ≈5–8 mmol/kg, while in the case of hemicarboaluminate sorption occurred also in the interlayer resulting in a sorption capacity of ≈1000 mmol/kg. The sorption on C-S-H was found one order of magnitude lower and increased with increasing Ca/Si as its uptake is promoted by the Ca-citrate surface complexes. The sorption coefficients of citrate measured on hydrated Portland cement were with R_d = 10–30 $L \cdot kg^{-1}$ comparable to the sorption observed on high Ca/Si C-S-H and AFm phases, underlining the strong uptake of citrate in hydrated cements.

1. Introduction

Citrate is used as additive in mortar industry to control setting and hardening of cementitious materials [1–4]. It is applied either as citric acid or as one of the alkali salts. It can act in Portland cement (PC) at high concentrations above ≈0.10–0.15 mass-% per cement as retarder [3] or at low concentrations below ≈0.10 mass-% per cement as accelerator [5]. Concentrations higher than ≈0.30–0.40 mass-% may lead to excessive retardation [3] and to the formation of calcium citrate [6]. Citrate is widely used as a retarder in calcium aluminate cements, calcium sulfoaluminate cements, magnesium sulfate and phosphate cements [1,2,7–11]. It has been observed that citrate slows down the dissolution of cement clinker but seems to accelerate ettringite formation in low dosages [3]. Citrate added disappears rapidly from the pore solution indicating an uptake of citrate by solid phases, although it remains unclear to which hydrates citrate is bound [3]. AFm phases bind a wide variety of different anions in their interlayer and their surface [12–15] such that they represent a potential sink for the immobilization of organic anions. In fact, Nguyen and co-authors [10] observed the presence of more AFm phases (in particular monosulfoaluminate) in ladle slag-gypsum (LSG) based binder samples containing 1 wt% or 2 wt % of citrate than in citrate free cements, which could indicate a preferential uptake of citrate in AFm phases.

The role of low molecular weight (LMW) organics such as citrate is also of relevance in the context of repositories for nuclear waste disposal. Besides its presence as cement additive, citrate has been extensively used in the nuclear industry as decontamination and separation agent. It is accordingly found in certain waste streams disposed of in underground repositories, in particular those for the disposal of low- and intermediate-level radioactive wastes (L/ILW). Citrate has been shown to form stable complexes with radionuclides [16], thus potentially affecting their solubility and sorption properties under repository conditions. It has been observed that the sorption of LMW organics containing only one functional group such as methanol, ethanol, formaldehyde, acetaldehyde, formic acid and acetic acid is generally very weak [17]. On the other hand, a significantly stronger uptake has been reported for polyhydroxocarboxylic acids such gluconic and isosaccharinic acids [3,18–21]. The structure of citrate with four potential donor sites (the central and two terminal carboxylic groups and the hydroxyl group in alpha position, see Fig. 1), makes it probable that it interacts strongly with cementitious phases.

The main hydrates formed in a Portland cement are calcium silicate

* Corresponding author at: Laboratory Concrete & Asphalt, Empa, Swiss Federal Laboratories for Materials Science and Technology, Überlandstrasse 129, 8600 Dübendorf, Switzerland.
E-mail address: rosa.guidone@kit.edu (R.E. Guidone).

https://doi.org/10.1016/j.cemconres.2023.107404
Received 9 December 2022; Received in revised form 31 October 2023; Accepted 3 December 2023
Available online 2 February 2024

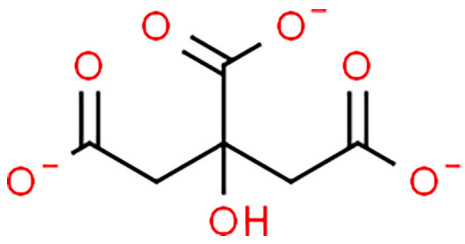

Fig. 1. Schematic structure of citrate.

hydrate (C-S-H[1]), portlandite, ettringite: AFt (Al_2O_3-Fe_2O_3-tri) phase and AFm (Al_2O_3-Fe_2O_3-mono) phases [22–24]. C-S-H, the major phase in hydrated Portland and blended cements, is poorly ordered and has a layered structure, with calcium oxide mainsheets connected on both sides to silica chains, which are arranged in *dreierketten* chains. Within the silica chains, the two "pairing" silica coordinate with Ca in the main layer, while the third tetrahedron, the bridging SiO_2 is connected to two pairing silica [25–28]. These layers are negatively charged and the interlayer between contains water as well as charge balancing cations [29]. The Ca/Si in C-S-H varies between 0.7 and 1.5 depending on the availability of CaO and SiO_2 in the system, and the availability of water influences its water content.

AFm phases have a layered double hydroxide (LDH) structure with positively charged main layers and an interlayer where anions and water are present. The main layer consist of sheets of $Ca(OH)_6$ in which one-third of Ca^{2+} sites are replaced by Al^{3+} (and/or Fe^{3+}) generating a positive net charge compensated by the interlayer anions. Different anions, such as SO_4^{2-}: monosulfoaluminate, Ms ($Ca_4Al_2O_6$-SO_4·12–16H_2O or C_4AsH_{12-16}), CO_3^{2-}: monocarboaluminate, Mc ($Ca_4Al_2O_6CO_3$·11H_2O or C_4AcH_{11}) or OH^- plus 0.5 CO_3^{2-}: hemicarboaluminate, Hc ($Ca_4Al_2O_6(CO_3)_{0.5}(OH)$·11.5$H_2O$ or $C_4Ac_{0.5}H_{12}$) can be hosted in the interlayer region [15,24,30–33].

Ettringite, $Ca_6[Al(OH)_6]_2(SO_4)_3$·26H_2O, present also in natural alkaline environments [34], occurs in cementitious system as a major hydrate phase. $[Al(OH)_6]^{3-}$ octahedra are linked together by calcium ions, which are surrounded by four water molecules, located in the outer surface of columnar units. Sulfate ions (SO_4^{2-}) and the remaining water molecules are present in the resulting channels and partly bound within the structure [35–37].

The present study aims to evaluate the uptake of citrate by the main cement hydrates: C-S-H, AFm phases, and ettringite based on the preparation of the citrate-AFm and citrate-ettringite phases, as well as on sorption experiments on monosulfoaluminate, monocarboaluminate, hemicarboaluminate, ettringite and C-S-H. Thermodynamic modelling is used to derive the solubility constants of the pure phases and to assess the formation of aqueous citrate complexes.

2. Materials and methods

2.1. Materials

All AFm phases were synthesized using tricalcium aluminate, C_3A: $Ca_3Al_2O_6$, as precursor. C_3A was prepared by mixing $CaCO_3$ (Merck Millipore, ≥98.5) and Al_2O_3 (Sigma-Aldrich, ≥99.0 %) at a 3:1 M ratio and by heating the mixture to 800 °C for 1 h, at 1000 °C for another 4 h and at 1425 °C for 24 h following the procedure applied by Nedyalkova et al. [13]. CaO was prepared by heating $CaCO_3$ at 1000 °C for 12 h, and cooling it down in a closed desiccator to minimize the CO_2 uptake. Trisodium citrate dihydrate ($Na_3C_6H_5O_7$·2H_2O, Sigma-Aldrich, ≥98.0 %) and NaOH (Merk, ≥98.0 %) solutions were prepared using high-purity deionized water (resistivity = 18.2 MΩcm) generated by a Milli-Q Gradient A10 System (Millipore, Bedford, USA).

To prepare citrate-AFm, C_3A, CaO and trisodium citrate dihydrate (Na_3-citrate) in molar ratio of 1:1:$^2/_3$ were mixed with high-purity deionized water at a solid-to-liquid-ratio (S:L) of 52 g·L^{-1} (S = 2.6 g and L = 0.05 L) to obtain $3CaO{\cdot}Al_2O_3{\cdot}Ca(C_6H_5O_7)_{0.67}{\cdot}nH_2O$. In order to investigate the reaction kinetics by using an excess of citrate ions and possible differences arising in the final product by using either Na and K–citrate salts as reagents, two additional samples with a 85 % surplus of citrate concentration (222 mM of citrate) and surplus of CaO were prepared at a S:L of 68 g·L^{-1} using either Na_3-citrate or K_3-citrate ($K_3C_6H_5O_7{\cdot}H_2O$, Sigma-Aldrich, ≥99.0 %). Monosulfoaluminate, monocarboaluminate and hemicarboaluminate were synthesized by mixing stoichiometric amounts of C_3A (1.35 g) and $CaSO_4$, $CaCO_3$, or 0.5 $CaCO_3$ + 0.5 CaO with 40 mL of high-purity deionized water. Different S:L ratio were applied for AFm phases in order to have in all preparation a constant C_3A content (for AFm phases) and Ca concentration equal to 0.02 mol·L^{-1}.

Citrate-AFt was prepared by mixing C_3A, Na_3-citrate, and CaO with molar ratio of 1:2:3 with deionized water (S:L = 62 g·L^{-1}) in order to obtain $3CaO{\cdot}Al_2O_3{\cdot}Ca_3(C_6H_5O_7)_2{\cdot}nH_2O$. Sulfate based ettringite (S:L = 42 g·L^{-1}), finalized for sorption experiments, was synthesized by mixing 0.6 g of CaO and 1.1 g of Al_2SO_4·16.3 H_2O (water content measured by TGA) in 40 mL of high-purity deionized water.

C-S-H phases with Ca/Si ratio of 0.8, 1.0, 1.2 and 1.4 and S:L of 55 g·L^{-1} were synthesized by mixing stoichiometric amounts of CaO and SiO_2 (Aerosil 200, Evonik, ≥99.8 %) with high-purity deionized water.

All samples were equilibrated for two months in closed PE bottles at 20 °C on horizontal shakers (100 rpm) before used for sorption experiments or further analysis.

Sorption experiments were also conducted on a hydrated (28 days) Portland cement (PC) paste. A CEM I 42.5 N was used. Cement paste was prepared by mixing 1 kg of anhydrous Portland cement (c) with 400 g of distilled water (w) (w/c = 0.4). The paste was stored in 0.5 L PE bottles under controlled conditions at 20 °C and after 28 days of hydration ground by hand to <63 μm. The sorption batch experiments were carried out by using 2.5 g of hydrated PC and a final solid to liquid ratio of 50 g·L^{-1} (see Section 2.3).

The composition of the unhydrated cement determined by X-ray fluorescence analysis (XRF) and the phase contents by quantitative X-ray

Table 1
Chemical-mineralogical composition of unhydrated and hydrated PC (CEM I 42.5 N).

XRF[d] (mass-%)		QXRD[e] (mass-%)		
Parameter	PC	Phase[c]	PC	hydrated PC
SiO_2	19.86	C_3S	58.3	10.0
Al_2O_3	4.86	C_2S	13.9	11.0
Fe_2O_3	2.88	C_3A cubic	2.4	0.5
Cr_2O_3	0.005	C_3A orthorh.	5.5	2.1
MnO	0.050	C_4AF	8.0	5.7
TiO_2	0.251	Lime	0.2	
P_2O_5	0.235	Portlandite	1.1	15.6
CaO	63.42	Gypsum	1.8	
MgO	1.55	Bassanite	2.1	
K_2O	0.85	Anhydrite	0.3	
Na_2O	0.15	Arcanite	0.5	
SO_3	3.18	Calcite	3.5	1.3
CO_2[a]	1.61	Dolomite	0.5	0.8
L.O.I.[b]	2.54	Quartz	0.5	0.5
		Ettringite		6.5
		Amorphous/other[c]		65.4

[a] Calculated from total carbon determined by combustion analysis.
[b] Loss on ignition.
[c] Includes C-S-H, hemi- and monocarboaluminate and further phases.
[d] The accuracy of the measurements is in compliance with EN 196–2 and ISO 10694, respectively.
[e] For accuracy of the measurements see [39,43–45].

[1] Cement notation is used: C = CaO, A = Al_2O_3, S = SiO_2, c = CO_2, s = SO_3, H=H_2O.

diffraction (QXRD) are reported in Table 1. Quantification was performed by Rietveld refinement using X'Pert Highscore Plus *V*. 4.8 following the procedure and using the structures recommended by [38]. The hydration of the paste was stopped by solvent exchange using the method by Snellings et al. [39] prior to analysis. The amorphous content in the hydrated paste was quantified using G-factor method [40,41] with CaF_2 (Sigma Aldrich, 99.9 %) as external standard and includes mainly C-S-H and AFm-phases. For the hydrated paste the results were referred to 100 g of unhydrated cement using the ignited sample mass at 550 °C as determined by thermogravimetric analysis [42].

2.2. Kinetic experiments

In order to investigate the citrate sorption as function of time, kinetic experiments were carried out at contacting times of 1, 2, 4, 7 and 14 days. To 40 mL of solution containing the pre-synthesized hydrates 5 mL of 1 M NaOH solution and 5 mL of H_2O and 0.49 g of Na_3-citrate were added in order to reach a total citrate concentration of 33 mM, a total Na concentration of 0.2 M and a total liquid volume of 50 mL. The samples were re-equilibrated in closed PE bottles on horizontal shakers (100 rpm) and at constant temperature (20 °C).

After the sorption experiments, the solid phases of AFm phase and ettringite were separated as described in the Section 2.3 and dried in a desiccator over saturated $CaCl_2$ solution (~35 % relative humidity) at room temperature from two to four weeks following the procedure outlined by Nedyalkova et al. [13]. The C-S-H phases were freeze-dried using liquid nitrogen following the procedure of L'Hôpital et al. [46] to minimize CO_2 uptake, kept under vacuum for 7 days to remove free water and then also stored in a desiccator over saturated $CaCl_2$ solution.

2.3. Sorption experiments

Sorption experiments were performed using the pre-synthesized phases and hydrated cement powder ($d_{particle} < 63$ μm) by adding different volumes (0.01–0.83 mL) of 0.02 M Na_3-citrate solution or 0.01 to 0.49 g $Na_3C_6H_5O_7.2H_2O$ in order to obtain citrate concentration from $2{\cdot}10^{-5}$ to 0.033 M citrate. Where needed, also 1 M NaOH solutions were added to reach in all cases a final Na concentration of 0.2 M (pH ~ 13.2) and 50 mL of solution. In the case of PC sorption experiments, a supplemental volume of Milli-Q water (40 mL) was used to achieve a final S:L of 50 $g{\cdot}L^{-1}$. The final monosulfoaluminate, monocarboaluminate, hemicarboaluminate suspensions have an S:L of 44 $g{\cdot}L^{-1}$, 37 $g{\cdot}L^{-1}$ and 35 $g{\cdot}L^{-1}$; ettringite and C-S-H suspensions of 32 $g{\cdot}L^{-1}$ and 44 $g{\cdot}L^{-1}$, respectively.

Specimens were re-equilibrated for 7 days at 20 °C on horizontal shakers (100 rpm). Separation of the solid and the liquid phase was carried out in N_2 filled glove boxes by vacuum filtration through 0.45 μm nylon filters. In order to preserve the solid phase, no washing was carried out during the filtration. Drying steps were done as detailed above in Section 2.2.

For the sorption experiments, relatively short equilibration times of 7 days were chosen to minimize possible re-crystallization processes. The term sorption is used in a broad sense to describe the uptake citrate on the surface or in the interlayer or channels of AFm, AFt or C-S-H phases as different interactions may occur between citrate in aqueous solution and cement particle [47]: (i) non-specific adsorption on the surface due to electrostatic interactions; (ii) selective adsorption on reactive surface sites or the interlayer of minerals or (iii) incorporation in the structure of the hydrates. The partitioning of citrate between the solid and the liquid phase is also described in terms of distribution coefficients, R_d:

$$R_d = \frac{C_{i,eq} - C_{i,0}}{C_{i,eq}} \cdot \frac{V}{m} \left[L{\cdot}kg^{-1}\right] \quad (1)$$

where $C_{i,eq}$ indicates the equilibrium concentration [$mol{\cdot}L^{-1}$] of citrate, $C_{i,0}$ the initial concentration [$mol{\cdot}L^{-1}$], m is the mass [kg] of sorbent (cement hydrate) and *V* is the total volume [L] of solution.

2.4. Solid phase characterization

After drying, the samples were characterized by X-ray powder diffraction (XRPD), thermogravimetric analysis (TGA), infrared spectrometry (FTIR) and zeta potential measurements (C-S-H phases and Ms). XRPD analyses for citrate-AFm, citrate-AFt, ettringite, AFm phases and PC were performed on a Panalytical X'Pert Pro MPD diffractometer with θ-θ geometry, using CuKα radiation (λ = 1.54184 Å) equipped with a solid X-Celerator detector. XRPD patterns were recorded at room temperature in the interval $5° < 2\theta < 70°$ with a step size of 0.017° (2θ) and a total counting time of ~2 s for each step. The XRPD characterization of C-S-H phases was achieved using PANalytical X'Pert Pro MPD diffractometer (CuKα radiation, λ = 1.54184 Å) with rotating sample stage in a θ-2θ configuration and equipped with X'Celerator detector. XRPD scans were recorded with step size of 0.013° 2θ and with a fixed divergence slit size (0.25° 2θ) and an anti-scattering slit (0.5° 2θ) on the incident beam.

TGA was carried out on a Mettler Toledo TGA/SDTA 851 instrument (Mettler Toledo, Switzerland) on ~30 mg of sample using a heating rate of 20 °C/min and a temperature range between 30 °C and 980 °C under N_2. The water losses are reported as mass of H_2O/mass of dried sample. Portlandite (CH) was quantified based on the weight loss in temperature range 400–500 °C using the tangential method as detailed in Lothenbach et al. [42]. The amount of CH was expressed relative to the mass of the samples at 600 °C.

FTIR spectra were recorded between 4000 cm^{-1} and 400 cm^{-1} with a resolution of 4 cm^{-1} on a Bruker Tensor 27 FT-IR spectrometer on powder samples to analyse the incorporation of citrate on the hydrates. The evolution of Ca to Si ratio of the C-S-H phases was calculated as a function of the citrate equilibrium concentration (reported in the ESM) by mass balance, Eq. (2):

$$Ca/Si_{solid} = \left([Ca]_{tot,in} - [Ca]_{tot,eq} - [Ca]_{portlandite}\right) \Big/ \left([Si]_{tot,in} - [Si]_{tot,eq}\right) \quad (2)$$

Zeta potential measurements were carried out using a Zeta Probe instrument (Colloidal Dynamics Inc., North Attleboro, MA) based on the electroacoustic method on stirred suspensions. An alternating high-frequency electric field was applied causing the oscillation of charged particle which generate sound waves. The instrument determines the dynamic mobility of charged particle present in a suspension, which is subsequently converted in zeta potential by the standard software. Prior to each measurement, pH meter (4.01, 7.01 and 10.01 standard solutions) and Zeta Probe instrument (KSiW, provided by Colloidal Dynamics Inc.) were calibrated. The zeta potential measurements were carried out at 23 °C in suspensions with a solid concentration of 4.8 wt% in a total volume of 270 mL.The suspensions were titrated with citrate solution (0.09 M) from $3.3 \cdot 10^{-4}$ M to $6.6 \cdot 10^{-3}$ M with a titration increment step of $3.3 \cdot 10^{-4}$ M. Milli-Q water was used as solvent for all suspensions measurement. The suspension was agitated in order to prevent sedimentation. The zeta potential of the background solutions was measured at the same conductivity for each solutions in a Teflon small volume static beaker. The zeta potential of each sample was recalculated accordingly by the software including the corresponding corrections as also detailed in [48,49].

2.5. Liquid phase characterization

The pH values were measured on an aliquot of the solution using a Knick pH-meter with a SE 100 pH/Pt 1000 electrode at room temperature. The instrument was calibrated with NaOH solution of known concentrations (0.1, 0.2, 0.5 and 1 M) to minimize the alkali error [50].

The total concentrations Al, Ca, Na, Si and S were measured on an Agilent 5110 ICP-OES equipped with an Agilent SPS 4 autosampler using

Argon as inert gas. The samples were diluted prior to analysis by a factor of 10, 100 and 1000 with 2 wt% HNO_3 solutions to prevent precipitation of any solids.

The total organic concentration was measured using a Sievers 5310C TOC analyser. The samples were diluted at least by a factor of 5 (for low organic concentrations) with 0.1 M HCl solution, and by a factor of 10, 100 and 1000 with 0.01 M HCl at higher organic concentrations.

2.6. Thermodynamic calculations

Thermodynamic calculations were carried out to obtain the solubility product of synthesized AFm-citrate and AFt-citrate based on the measured concentrations. The thermodynamic modelling program GEM-Selektor (GEMS) [51] was used, which takes into account chemical interactions involving solids, solid solutions, metal ions, and aqueous electrolyte at once. General thermodynamic data were taken from the NAGRA/PSIi database [16], data for cement hydrates from the Cemdata18 database [52]. The CSHQ model [52,53] was used to describe the alkali uptake and the composition of C-S-H.

The complexation of citrate with the different cations was considered using the complex formation constants from [16,54–56] as detailed in Table 2.

Activity coefficients of the aqueous species were calculated with the built-in extended Debye-Hückel equation and NaOH as a background electrolyte:

$$log\gamma_i = \frac{-A_y z_i^2}{1 + B_y a_i \sqrt{I}} + bI$$

z_i is the charge of species i, I is the effective molal ionic strength, a_i = 3.31, is a parameter dependent on the size of ion i, b corresponds to 0.98 in NaOH [59,60], and A_y and B_y are P,T-dependent Debye-Hückel solvent parameters.

The solubility products and saturation indices were calculated from the activity of the species Ca^{2+}, $Al(OH)_4^-$, OH^-, SO_4^{2-}, CO_3^{2-}, $C_6H_7O_5^{3-}$ and H_2O, obtained using GEMS based on the measured total concentrations.

3. Results

3.1. Synthesized reference phases

3.1.1. Sulfate, carbonate and citrate containing AFm phases

Ms, Mc, Hc, ettringite as well as citrate containing AFm and AFt phases were synthesized as references. AFm phases have a layered structure consisting of positively charged main layers, $[Ca_4Al_2(OH)_{12}]^{2+}$, and anions and water present in the interlayer region, $[X_x{\cdot}nH_2O]^{2-}$, such that the formation of a citrate-containing AFm phase and substitution of the already existing interlayer anion seem plausible. AFm phases form hexagonal or pseudo hexagonal crystals: monosulfoaluminate and hemicarboaluminate (abbreviated as Ms and Hc respectively) crystallize in trigonal geometry [61,62], while monocarboaluminate has a triclinic symmetry.

Fig. 2 provides the XRPD patterns of the reference phases. For well-crystalline solid phases, XRD allows to identify the unit cell dimensions of phases by determination of the position of the main basal reflection (at low 2θ degrees: 7°-10°; Ms: $d_{(003)}$ = 8.9 Å, Mc: $d_{(001)}$ = 7.9 Å, Hc: $d_{(006)}$ = 8.3 Å) and relative to the direction hkl (00×). Characteristic of the AFm phases family is also the presence of a reflection at ≈31° 2θ ($d_{(110),\ Ms} \approx d_{(110),\ Mc}$ = 2.8 Å; $d_{(110),\ Hc}$ = 2.9 Å) related to the plane (110).

Ms is characterized by a (003) reflection at ≈9.9° 2θ (8.9 Å) indicating the presence of mainly $Ca_4Al_2(SO_4)(OH)_{12}{\cdot}6H_2O$ (C_4AsH_{12}) after drying. Additionally, a smaller reflection appears at ≈9.4° 2θ (7.9 Å), indicating some C_4AsH_{14}, the hydrated form of monosulfoaluminate predominant in suspension, being present [63].

Hc is characterized by a (006) reflection at 10.7° 2θ (8.3 Å) indicating the formation of $Ca_4Al_2(CO_3)_{0.5}(OH)_{13}{\cdot}5.5H_2O$. In the Hc system, a secondary phase tentatively assigned to carbonated

Table 2
Thermodynamic data used to investigate citrate-complexes. (H_3Cit = citric acid).

Species	Reaction	log $\beta^0_{m,I}$	Reference
Aqueous complexes[a]			
$HCit^{2-}$	$Cit^{3-} + H^+ \leftrightarrows HCit^{2-}$	6.36	[16]
H_2Cit^-	$HCit^{2-} + H^+ \leftrightarrows H_2Cit^-$	4.78	[16]
H_3Cit^0	$H_2Cit^- + H^+ \leftrightarrows H_3Cit^0$	3.13	[16]
$CaCit^-$	$Ca^{2+} + Cit^{3-} \leftrightarrows CaCit^-$	4.80	[16]
$CaHCit^0$	$Ca^{2+} + HCit^{2-} \leftrightarrows CaHCit^0$	2.92	[16]
CaH_2Cit^+	$Ca^{2+} + H_2Cit^- \leftrightarrows CaH_2Cit^+$	1.53	[16]
$KCit^{2-}$	$K^+ + Cit^{3-} \leftrightarrows KCit^{2-}$	1.42[b]	[54]
K_2Cit^-	$2\,K^+ + Cit^{3-} \leftrightarrows K_2Cit^-$	1.93[b]	[54]
$NaCit^{2-}$	$Na^+ + Cit^{3-} \leftrightarrows NaCit^{2-}$	1.54[b]	[54]
Na_2Cit^-	$2Na^+ + Cit^{3-} \leftrightarrows Na_2Cit^-$	2.38[b]	[54]
$AlHCit^+$	$Al^{3+} + Cit^{3-} + H^+ \leftrightarrows AlHCit^+$	12.90	[55,56]
$AlCit^0$	$Al^{3+} + Cit^{3-} \leftrightarrows AlCit^0$	9.90	[55,56]
$AlCitOH^-$	$Al^{3+} + Cit^{3-} + H_2O \leftrightarrows AlCitOH^- + H^+$	8.10	[55,56]
$Al(Cit)_2^{3-}$	$Al^{3+} + 2Cit^{3-} \leftrightarrows AlCit_2^{3-}$	14.13	[55,56]
$Al(Cit)_2(OH)^{4-}$	$Al^{3+} + 2Cit^{3-} + H_2O \leftrightarrows Al(Cit)_2(OH)^{4-} + H^+$	10.19	[55,56]
$Al_3(Cit)_3(OH)_4^{4-}$	$3Al^{3+} + 3Cit^{3-} + 4H_2O \leftrightarrows Al_3(Cit)_3(OH)_4^{4-} + 4H^+$	20.6	[55,56]
Solids			
$H_3Cit(H_2O)$(cr)	$H_3Cit(H_2O)(cr) \leftrightarrows H_3Cit^0 + H_2O$	1.33	[16]
$Ca_3Cit_2(H_2O)_4$(cr)	$Ca_3Cit_2(H_2O)_4(cr) \leftrightarrows 3Ca^{2+} + 4H_2O + 2Cit^{3-}$	−17.9	[16]

[a] Sari [57] suggested the formation of $CaH(Cit)_2^{3-}$, $Ca(Cit)_2^{4-}$ and $CaH_{-1}Cit^{2-}$ complexes, but did not give any details on the concentrations used, on the fitting procedure and did not report the experimental data, thus those data were not included in the present calculations following the recommendation in the NEA-TDB review on organics [16]. A recent study of Gácsi et al. [58] indicated that the formation of $CaH_{-1}Cit^{2-}$ is expected to be relevant only for very high pH values (pH > 15).

[b] The NEA-TDB review on organics [16] suggested the use of SIT interaction coefficients to describe the interaction between Na^+ or K^+ with Cit^{3-} at high ionic strength. As in the present work the extended Debye-Hückel was used and ionic strength was in all cases below 0.5 M, complexation constants were used. In all cases <0.1 % of total Na, K, or citrate in solution were present in those complexes and their consideration had a negligible effect on the calculated solubility products (<0.01 log units).

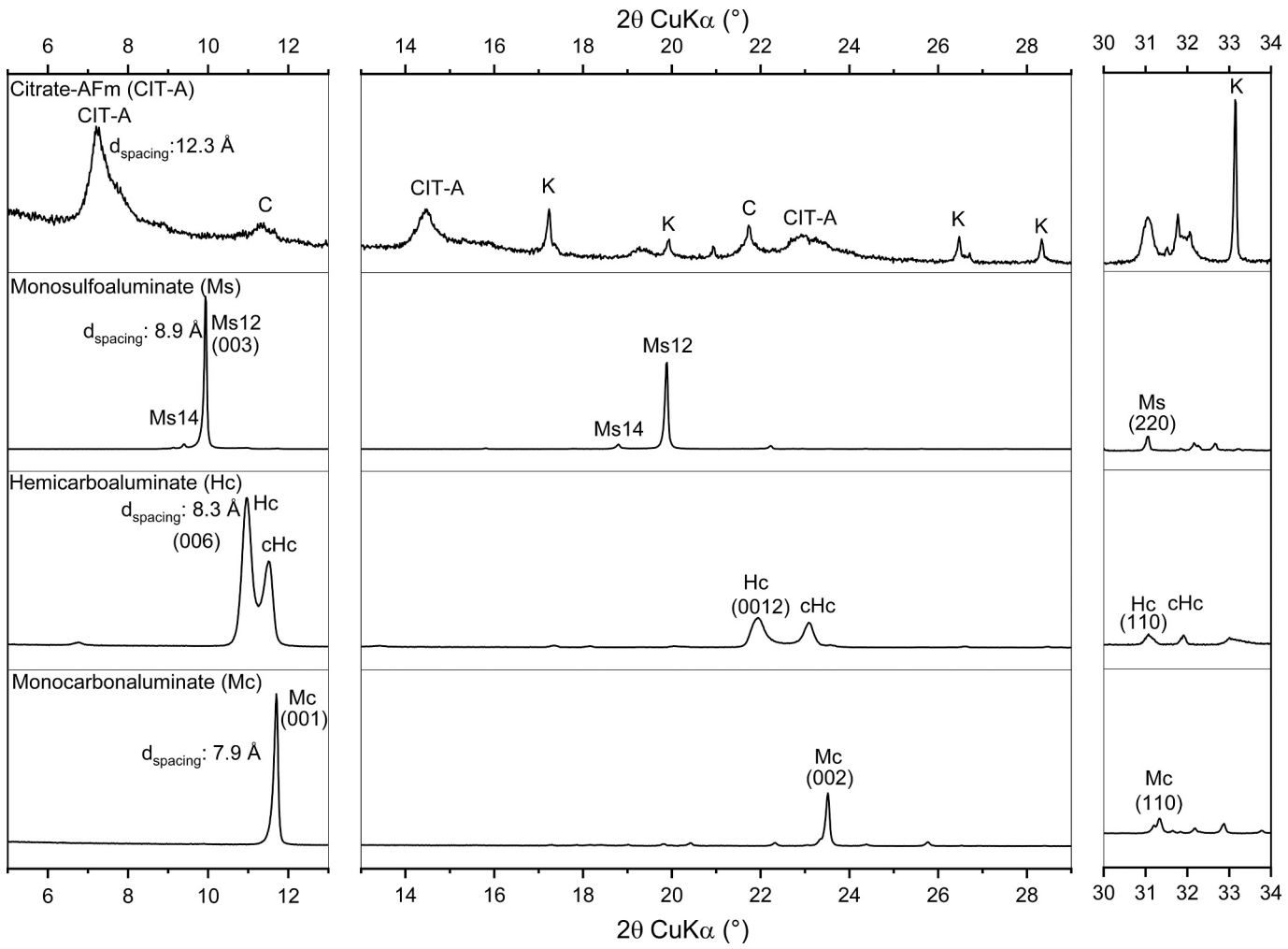

Fig. 2. XRPD pattern diffraction of synthesized citrate-AFm, Ms, Hc, and Mc after 2 months of equilibration time. C: calcium citrate ($Ca_3(C_6O_5H_7)_2{\cdot}4H_2O$); Cit-A: citrate-AFm; cHc: carbonated hemicarboaluminate; Hc: hemicarboaluminate; K: katoite ($Ca_3Al_2(OH)_{12}$); Mc: monocarboaluminate (C_4AcH_{11}); Ms12: monosulfoaluminate-12 (C_4AsH_{12}); Ms14: monosulfoaluminate-14 (C_4AsH_{14}).

hemicarboaluminate, $C_4Ac_{0.8}H_{10.2}$ [64] (cHc) was also detected.

As member of AFm phases, monocarboaluminate with a triclinic structure (Mc, C_4AcH_{11}) is defined by a repetitive sequence of $[Ca_2Al_2(OH)_{12}]^{2+}$ layers and an interlayer region ($2H_2O$-$[CO_3{\cdot}3H_2O]^{2-}$) in which the CO_3^{2-} anions are bound to the main layer Ca via shared oxygen bonds resulting in a very rigid structure and a narrow interlayer distance of 7.9° Å (001) [32,65].

The XRPD pattern of citrate-AFm indicates the presence of a layered structure with a high intensity reflection at 7.2° 2θ corresponding to a basal spacing d = 12.2 Å ((hkl) = (003)), which is in agreement with the values reported by [66] for tetracalcium aluminate hydrate phases (C_4AH_{19}) equilibrated with increasing citrate concentrations ($0 \leq x_{mol,\ citrate} \leq 0.66$). The reflection at ≈14.5° 2θ (6.1 Å) is related to the basal spacing (006) as well as the less intense, partially overlapped reflection at ≈23° 2θ ($d_{spacing}$ = 4.0 Å), which is likely correlated to the (009) reflection. The broad reflection shapes indicate an only poorly ordered citrate-AFm structure as previously reported by [66]. For trigonal AFm structures such as monosulfoaluminate and hemicarboaluminate, a main layer reflection (110) at 31.03° 2θ [67] is characteristic, while for monoclinic monocarboaluminate it is shifted to ≈32° 2θ. In the case of citrate-AFm this main layer reflection is overlapped by the reflections of katoite ($Ca_3Al_2(OH)_{12}$). In addition, some ill-ordered $Ca_3(Cit)_2(H_2O)_4$ (main reflections at 11 and 22° 2θ) was observed as also reported by [66]. The presence of katoite indicates a lower stability of citrate-AFm, as compared to that of e.g. monosulfoaluminate or monocarboaluminate (Fig. 2). Furthermore, traces of tricalcium aluminate ($Ca_3Al_2O_6$) indicate the incomplete conversion of initial reagents used for the synthesis. An increase of the basal spacing compared to AFm phases containing sulfate or carbonate can be expected due to the larger size of citrate compared to carbonate or sulfate ions, as previously observed for different organic containing AFm phases [68–70]. For citrate containing Mg/Al layered double hydroxide (LDH) phases, which have similar to AFm phases a positively charged main layer and an interlayer containing anions and water, a comparable basal spacing of d = 11.8 to 12.0 Å [71,72] was reported. Zhang et al. [71] postulated a perpendicular orientation of citrate molecules in Mg-LDH resulting in "pillared" LDH. Although the linkage of two main layers by the terminal carboxylate groups in citrate is a possible coordination mode, also a 5-bond ring structure formed by coordination of a carboxylate and the deprotonated α-hydroxyl group with calcium could be possible as observed by [73] for citrate sorbed on calcite.

Thermogravimetric analysis (TGA) has been used to determine the amount of water associated with the different AFm phases, see Fig. S1 in the Electronic Supplementary Material (ESM). The water loss in the temperature range 30–550 °C has been assigned to interlayer water (below 250 °C) and main layer water (250 to 550 °C) [42]. For Mc, Hc, and Ms the combined interlayer and main layer weight loss was found of ≈30–34 wt% in agreement with expected values [42]. The water loss region of citrate-AFm was less structured than those of the other AFm phases, which underlines the poorly ordered structure of citrate-AFm.

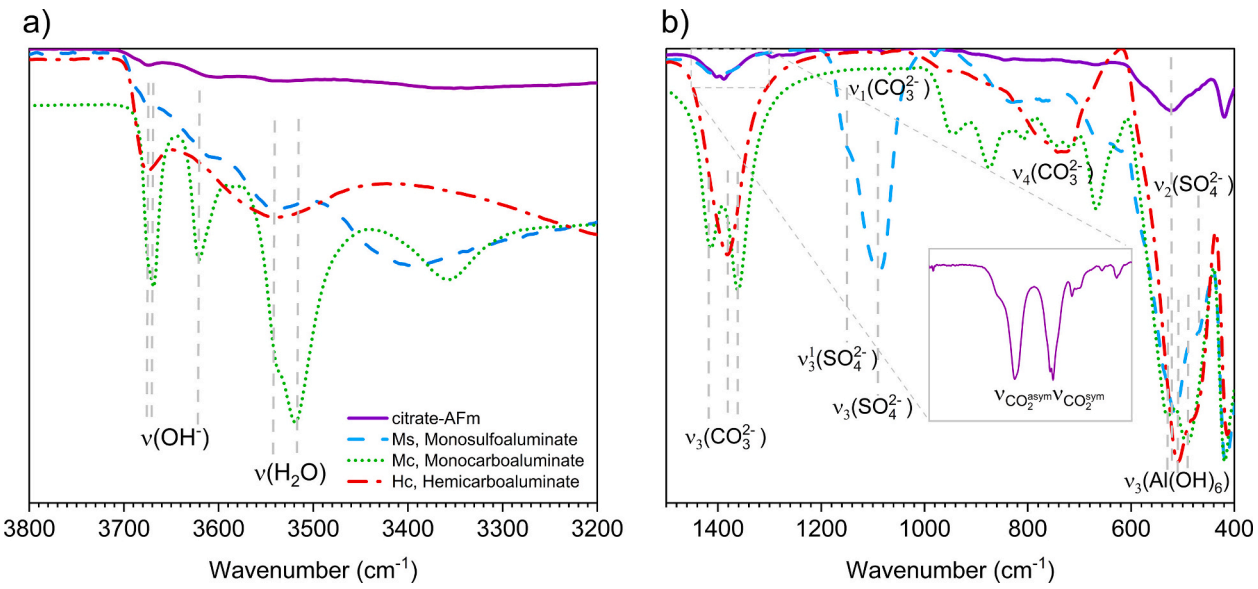

Fig. 3. FTIR spectra of the synthesized AFm phases in the frequencies ranges of (a) the hydrogen bond region (3800–3200 cm^{-1}) and (b) the interlayer anions (1500–400 cm^{-1}).

The weight loss at ≈300 °C (Fig. S1 in the ESM) might be caused both by the water loss of citrate-AFm as well by the water loss of katoite as detected by XRPD analysis [42]. Due to the presence of several other hydrates (citrate-AFm, katoite and $Ca_3(C_6H_5O_7)_2{\cdot}4H_2O$) with overlapping water loss regions in TGA (see ESM) the determination of the water loss was difficult. The comparison of the different water losses determined in the samples with a surplus of Na_3-citrate (see Fig. S2 in the ESM; corresponding XRPD patterns in Fig. S3) allowed to derive a water content of 12 water molecules as for monosulfoaluminate, with main water loss signals at 190 and 250 °C, while the weight loss due to citrate occurred around 800 °C.

FTIR analysis can be used to study the sorption of anions such as citrate to the interlayer or to the outer main layer. While sulfate, SO_4^{2-}, dissolved in water has a high-symmetry and only the vibration modes ν_1 and ν_3 are visible [74], the sorption of sulfate on a surface, such as on calcium present in the main layer of AFm phases lowers the symmetry of the sulfate leading to the splitting of the vibration mode ν_3 in two components [13]. In fact, the FTIR spectrum of Ms clearly shows the two

Table 3
Measured pH (measurement error ± 0.1 pH units), Na, K, Ca, Al, sulfate, carbonate (measurement error ± 5 %) and citrate (measurement error ± 7 %) content for pure AFm phases and citrate-AFm phase, used to calculate the ionic activity products (IAP) at 20 °C. The solubility products of pure phases available in literature at 25 °C are reported for comparison in the second last column.

Phases observed[a]	pH	Na (K)	Ca	Al	Sulfate	Carbonate	Citrate	IAP[b]	*log K°s*[c]
			— [mM] —					(this study)	
Ms, monosulfoaluminate: $Ca_4Al_2(SO_4)(OH)_{12}{\cdot}8H_2O \rightarrow 4Ca^{2+}+2Al(OH)_4^- + SO_4^{2-} + 4OH^- + 8H_2O$									
Ms	13.2	220	0.30	1.9	1.0	–	–	−30.21 ± 0.15[d]	−29.26 [77]
Mc, monocarboaluminate: $Ca_4Al_2(CO_3)(OH)_{12}{\cdot}5H_2O \rightarrow 4Ca^{2+} +2Al(OH)_4^- + CO_3^{2-} + 4OH^- + 5H_2O$									
Mc, Cc	13.4	216	0.55	0.15	–	0.38[e]	–	−32.00 ± 0.15[d]	−31.47 [77]
Hc, hemicarboaluminate: $Ca_4Al_2(CO_3)_{0.5}(OH)_{13}{\cdot}5.5H_2O \rightarrow 4Ca^{2+} +2Al(OH)_4^- + 0.5CO_3^{2-} + 5OH^- + 5.5H_2O$									
Hc, Mc	13.2	218	1.8	0.15	–	0.016[f]	–	−29.26 ± 0.17[d]	−29.13 [77]
Citrate-AFm[g]: $Ca_4Al_2(C_6H_5O_7)_{2/3}(OH)_{12}{\cdot}6H_2O \rightarrow 4Ca^{2+}+2Al(OH)_4^- + {}^2/_3(C_6H_5O_7)^{3-} + 4OH^- + 6H_2O$									
Cit-A, K, CA, C	13.3	213	0.69	6.1	–	–	1.5	−27.94	–
Cit-A, K, CA, C	13.1	213	5.1	0.90	–	–	12.7	−27.91	–
Cit-A, Cit-E, C	13.4	265	152	6.9	–		20.5	−27.86	–
Cit-A, CH	13.7	671	0.42	4.03	–	–	37	−29.98	–
Cit-A, CH, KC	13.8	(697)[h]	2.81	1.08	–	–	49	−27.80	–
Mean								−28.3 ± 2.8[i]	

[a] C: $Ca_3(C_6H_5O_7)_2{\cdot}4H_2O$; CA: tricalcium aluminate; Cit-A: citrate AFm; Cc: calcite; CH: portlandite; Ms: monosulfoaluminate; Mc: monocarboaluminate; Hc, hemicarboaluminate; K: katoite, KC: potassium citrate monohydrate.
[b] Ion activity product calculated in this study.
[c] log $K°_S$ reported by [77] for comparison.
[d] Mean of citrate free sample and samples containing ≤0.02 mM citrate.
[e] Assuming saturation with respect to calcite [77].
[f] Assuming saturation with respect to monocarboaluminate [77].
[g] d-spacing 12.27 Å, molar volume 424 cm^3/mol (trigonal structure).
[h] Value in the brackets correspond to the total potassium concentration is solution.
[i] Uncertainties were calculated as three times the standard deviations of the mean value (3σ).

vibration bands: ν_3 at ≈1100 cm^{-1} and ν'_3 at ≈1150 cm^{-1}. The latter band is visible as a shoulder of ν_3 (Fig. 3). The vibration bands ν_2 and ν_4 are observed at ≈460 cm^{-1} and at ≈980 cm^{-1} respectively. In the case of monocarboaluminate (Mc), where the interlayer anion CO_3^{2-} is bound to the main layer [32], the stretching vibration ν_1 is observed at ≈ 1070 cm^{-1}, while the absorption band for hemicarboaluminate (Hc) (the carbonate group is only weakly bond in the interlayer) occurs at ≈1090 cm^{-1} [75]. The weakly bound carbonate in Hc shows single signals for the bending vibration ν_4 at ≈750 cm^{-1} and ν_3 at ≈1400 cm^{-1}, while the bound carbonate with the resulting lower symmetry in Mc shows several signals in those regions in agreement with the observations of Nedyalkova and co-authors [13]. The absorption bands from 3000 cm^{-1} to 3600 cm^{-1} are related to OH^- stretching vibrations resulting from the interlayer water. The bands of Mc are narrower than those of Hc or Ms indicating more coordinated interlayer water in Mc. The main OH^- signal of Ms occurs at lower wavenumber than that of Hc indicating more coordinated water in Ms than in Hc. This is also in agreement with the three well-defined water loss areas observed by TGA for Ms (see ESM).

Citrate-AFm shows less intense FTIR signals than the other AFm phases, which is probably related to its poorly ordered structure as evidenced by the XRD characterization. As for all the other AFm phases, a signal ν_3 of $Al(OH)_6$ can be observed at ≈550 cm^{-1} and the presence of citrate is visible by the typical asymmetric (≈1600 cm^{-1}) and symmetric (≈1400 cm^{-1}) stretching modes of the carboxylate groups which occur generally in the wavenumber range 1600–1300 cm^{-1}(Fig. 3b) of carboxylic anions coordinated to metal ions [76].

The total concentrations measured for the different elements in the aqueous solution (see Table 3) were used to calculate the ion activity products (IAP) for monosulfoaluminate, monocarboaluminate, hemicarboaluminate as well as for citrate-AFm. The calculated ion activity products (IAP) of monosulfoaluminate, monocarboaluminate, hemicarboaluminate are comparable to those reported in [77,78] as indicated in Table 3. The solubility product, log K°_S, of citrate-AFm is comparable to monosulfoaluminate and hemicarboaluminate, but higher than that of monocarboaluminate. Although the value of the solubility product is comparable due to the different number of anions in the dissolution equations, the solubility of citrate-AFm is higher than that of monosulfoaluminate and hemicarboaluminate, as also evidenced by the higher ion concentrations and the formation of katoite in the presence of citrate-AFm.

3.1.2. *Sulfate and citrate containing ettringite*

The ettringite structure consists of $[Ca_6[Al(OH)_6]_2{\cdot}24H_2O]^{6+}$ columns surrounded by channels containing sulfate ions and water [37]. The sulfate ions in these channels can be replaced by other anions such as CrO_4^{2-}, SeO_4^{2-}, MoO_4^{2-}, or $B(OH)_4^-$ [79–83], such that also a replacement by small organic molecules such as citrate seems possible. The XRPD patterns of the prepared citrate-AFt and of sulfate based ettringite are shown in Fig. 4. The pattern of (sulfate-) ettringite is characterized by narrow well defined reflections including a main (100) signal at 9.7 Å in *a* direction (perpendicular to the columns) and a small (002)

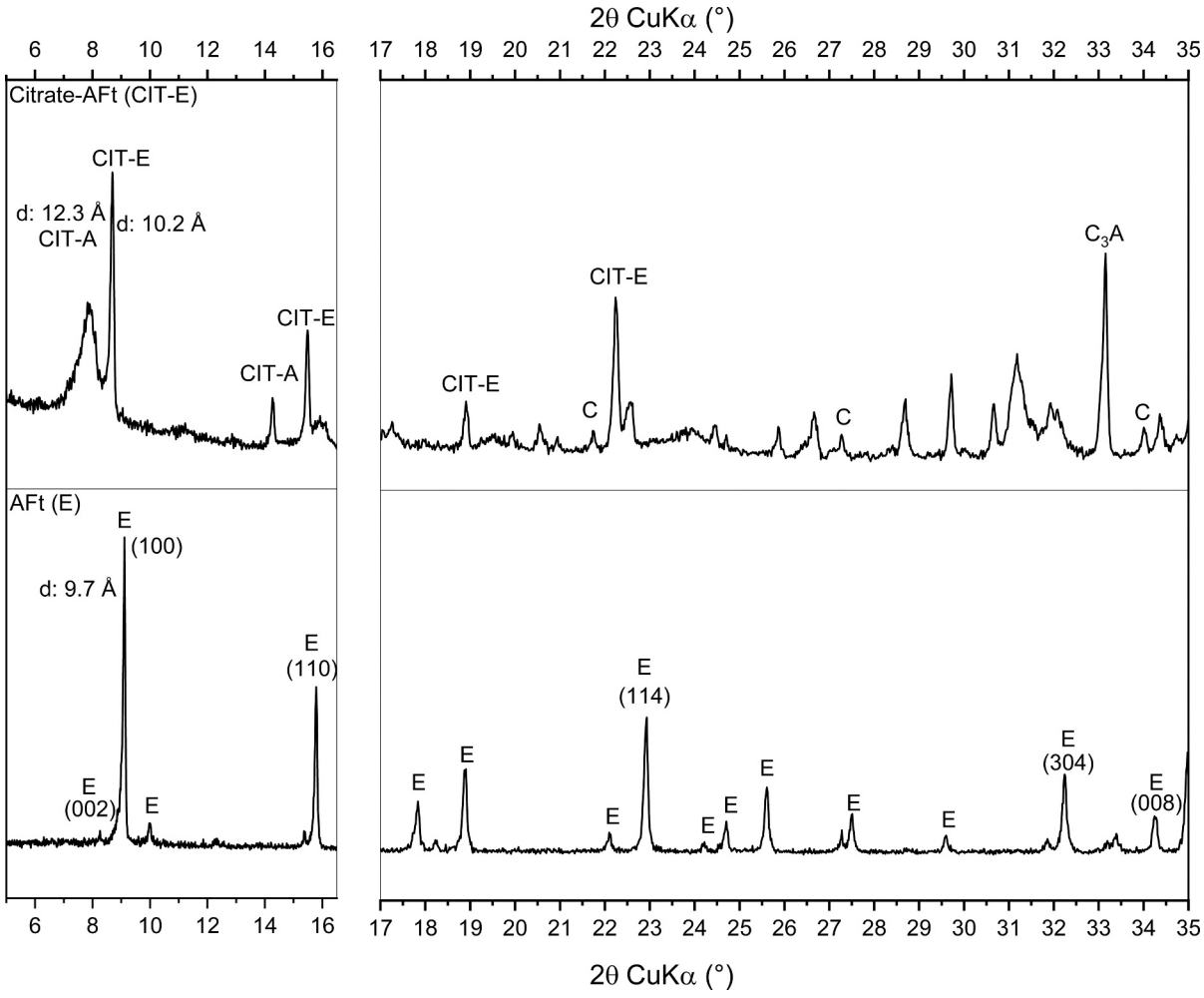

Fig. 4. XRPD pattern diffraction of citrate-AFt and sulfate-AFt after 2 months of equilibration time. Cit-E: citrate-ettringite, Cit-A: citrate-AFm, C: calcium citrate: $Ca_3(C_6O_5H_7)_2{\cdot}4H_2O$, C_3A: tricalcium aluminate: $Ca_3Al_2O_6$, E: (sulfate-)ettringite.

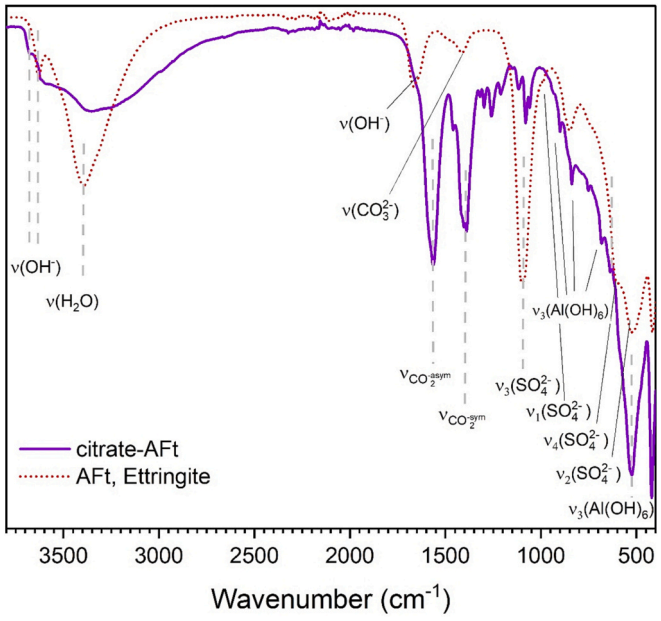

Fig. 5. FTIR spectra of the synthesized ettringite samples in the wavenumber region (3800–400 cm^{-1}).

reflection (parallel to the column) at 10.7 Å. The XRPD spectrum of citrate-ettringite is characterized by two main reflections between 7° to 9° 2θ ($d_{Cit\text{-}A}$ = 12.3 Å, $d_{Cit\text{-}E}$ = 10.2 Å) indicating the presence of two phases. The broad reflections are associated with citrate-AFm with a basal spacing of 12.3 Å as shown in Fig. 2. The reflections of citrate-AFt are much narrower with a main (100) signal at 10.2 Å, and a very small (002) reflection again at 10.7 Å in c-direction. The substitution of sulfate by citrate is expected to increase the distance along the a-axis (x00, perpendicular to the columns) as in fact observed for citrate-AFt (Fig. 1). In addition, unreacted tricalcium aluminate due to the strong retardation of the C_3A dissolution reaction by citrate as well as calcium citrate are observed. Unreacted C_3A was also observed in a 2nd preparation equilibrated for 4 months.

The TGA data (Fig. S4 in the ESM) indicated for sulfate containing ettringite a weight loss of 43 wt% with a main weight loss at 110 °C, which is near to the theoretical weight loss of 46 wt% expected for $Ca_6Al_2(SO_4)_3(OH)_{12}{\cdot}26H_2O$ [42]. The weight loss of citrate-AFt is with 44 wt% somewhat lower than the theoretical weight loss of 46 wt% for $Ca_6Al_2(C_6O_5H_7)_2(OH)_{12}{\cdot}26H_2O$, due to the presence of some citrate-AFm in the sample.

The FTIR analysis (Fig. 5) shows OH^- stretching vibrations of Al $(OH)_6^{3-}$ units at ≈3650 cm^{-1} for ettringite, [84] and at 3680 cm^{-1} for citrate-AFt. For ettringite the symmetric stretching vibration of H_2O with a maximum at ≈3390 cm^{-1} is well visible, while the H_2O signals for citrate AFt are more broadly distributed indicating the presence of less well ordered water. The bending vibrations of hydroxyl groups related to Ca-OH and to the intra-channel water, are visible for the ettringite sample at 1660 cm^{-1} and 1633 cm^{-1} [84], and those of the Al-OH group at ≈880 cm^{-1} and 850 cm^{-1}. The sulfate group generates two symmetric stretching vibrations ν_1 and ν_3 at 1090 cm^{-1} and 989 cm^{-1} [84,85]. The broad bands at ≈530 cm^{-1} and ≈610 cm^{-1} have been assigned by Myneni et al. [84] and Scholtzová et al. [85] to SO_4^{3-} symmetric and asymmetric bending vibrations (ν_2 and ν_4). Generally, these bands are difficult to distinguish due to the overlapping with Ca/Al-OH bending vibrations. The citrate-AFt spectrum shows also the bending vibrations of the hydroxyl group related to Ca-OH at 1660 cm^{-1} and the Al-OH stretching vibrations at 550 cm^{-1}, intensified by the Al-OH vibrations from the citrate-AFm phase. The signal at 1600 and 1400 cm^{-1} is again assigned to asymmetric and symmetric carboxylate stretching vibrations of the citrate group, of citrate in AFm (Fig. 3b) and citrate in the AFt channels.

The concentration of the aqueous solution in equilibrium with ettringite and citrate-AFt (see Table 4) were used to calculate the ion activity products (IAP) for sulfate-ettringite and citrate-AFt. The IAP of citrate-AFt is very similar to the solubility product of pure ettringite [78], indicating a lower stability of citrate-AFt than that of ettringite due to lower number of anions in the dissolution equations, as also evidenced by the higher ion concentrations and the formation of additional solids in the presence of citrate-AFt.

3.1.3. Calcium silicate hydrate (C-S-H) phases

The XRPD patterns of C-S-H phases prepared in 0.2 M NaOH with Ca/Si 0.8, 1.0, 1.2 and 1.4 are shown in Fig. 6. In all cases mainly C-S-H is present, at Ca/Si 1.2 and 1.4 in addition some portlandite is detected due to the high hydroxide concentration (200 mM NaOH) in agreement with the observations of [86]. The basal reflection related to the d-spacing (002) of C-S-H at ≈8 Å shifts towards higher 2θ values with the increase of the Ca content in C-S-H, which enhances the attractive forces between the negatively charged main layer and the positive charged interlayer region [87,88]. The broad reflection at ≈17 Å, assigned to the reflection (101) and visible only for Ca/Si of 0.8 and 1.0, indicates the occupation of the bridging Si-sites within the silica chains [86,87]. TGA (see Fig. S5 in the ESM) indicates a water loss of C-S-H of ≈0.20 g H_2O per g dry weight, which agrees well with the data reported elsewhere [46,86].

Fig. 7 shows the FTIR characterization of the C-S-H prepared, representing at 1400–800 cm^{-1} Si—O stretching and at 800–400 cm^{-1} binding vibrations. The main band at 950 cm^{-1} corresponds to several overlapping Si—O stretching bands. As observed previously [86] the

Table 4
Measured pH (measurement error ± 0.1 pH units), Na, K, Ca, Al, sulfate (measurement error ± 5 %) and citrate (measurement error ± 7 %) content for pure ettringite and citrate-AFt, used to calculate the ionic activity products (IAP) at 20 °C. The solubility products of pure phases available in literature at 25 °C are reported for comparison.

Phases observed[a]	pH	Na (K)	Ca	Al	Sulfate	Citrate	IAP[b]	$\log_{10} K°_S$[c]
			—[mM]—				(this study)	
AFt, ettringite: $Ca_6Al_2(SO_4)_3(OH)_{12}{\cdot}26H_2O \rightarrow 6Ca^{2+}+2Al(OH)_4^- + 3SO_4^{2-} + 4OH^- + 26H_2O$								
E	13.1	205	0.09	6.87	11.61	–	−45.42 ± 0.30[d]	−44.9 [77,78]
Citrate-AFt[e]**:** $Ca_6Al_2(C_6H_5O_7)_2(OH)_{12}{\cdot}26H_2O \rightarrow 6Ca^{2+}+2Al(OH)_4^- + 2(C_6H_5O_7)^{3-} + 4OH^- + 30H_2O$								
Cit-A, Cit-E, C	13.4	265	152.3	6.9	–	20.5	−41.1 ± 2.8[f]	this study

[a] C: $Ca_3(C_6H_5O_7)_2{\cdot}4H_2O$; Cit-A: citrate AFm; Cit-E: Citrate AFt; E: ettringite.
[b] Ion activity product calculated in this study.
[c] log $K°_S$ reported in literature at 25 °C for comparison.
[d] Mean of citrate free sample and samples containing ≤0.02 mM citrate.
[e] (100) unit-cell dimension 10.16 Å, molar volume 775 cm^3/mol (hexagonal structure).
[f] Error for citrate AFt calculated assuming an analytical error of 5 % in the measured concentrations.

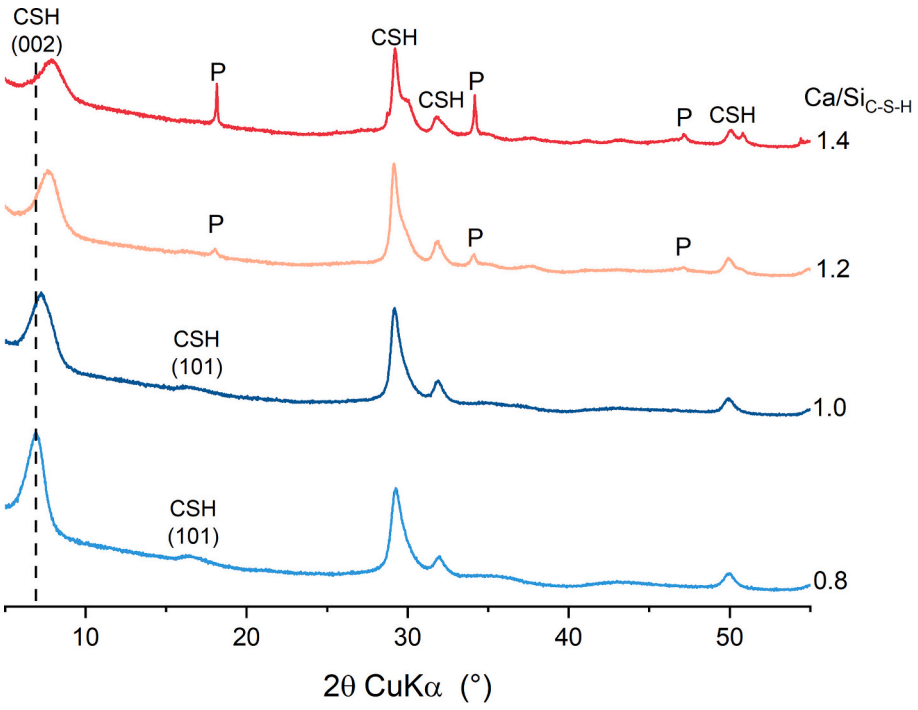

Fig. 6. XRPD of C-S-H phases synthesized with a Ca/Si ratio of 0.8, 1.0, 1.2 and 1.4 and equilibrated for 2 months. CSH: C-S-H; P: portlandite.

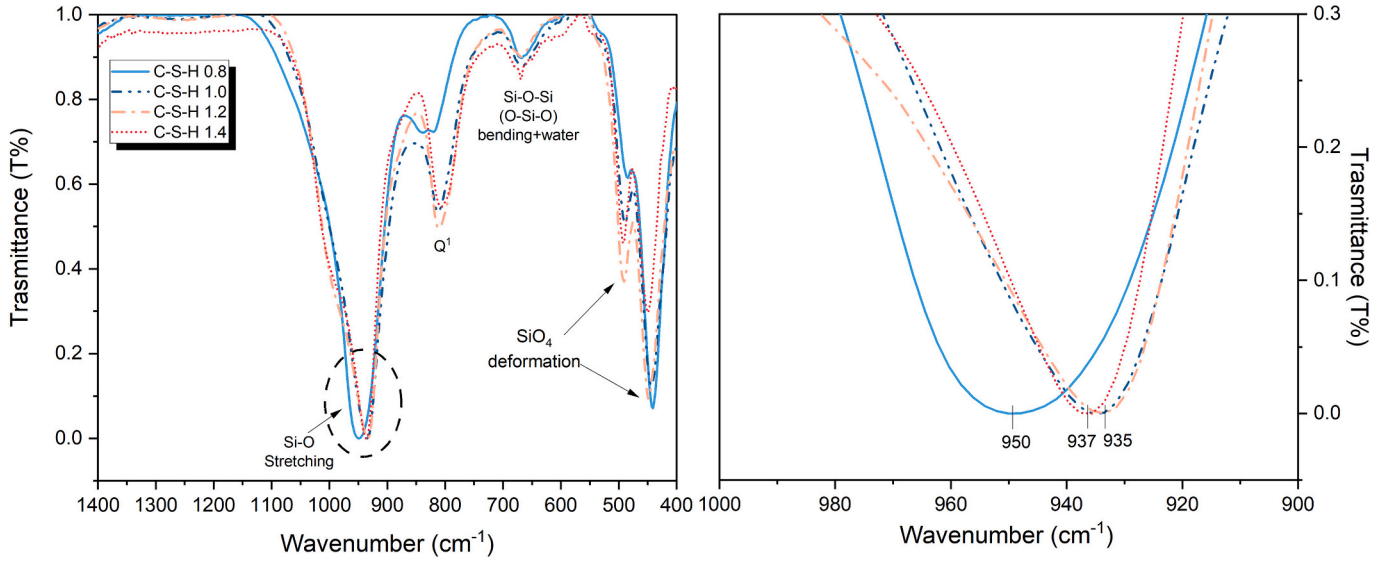

Fig. 7. FTIR spectra of C-S-H phases with a Ca/Si ratio of 0.8, 1.0, 1.2 and 1.4 in the wavenumber region (1400–400 cm^{-1}).

position of the main band shifts towards lower wavenumbers with increasing Ca/Si ratio, as consequence of the depolymerisation of the silica chain. No significant difference is observed between C-S-H Ca/Si = 1.2 and 1.4 where portlandite is present. The signal at 810 cm^{-1} refers to the stretching vibrations of the chains-end-sites of the silica tetrahedral, i.e. to Q^1 silica [86,89], as well as the bending vibrations at 500 cm^{-1}. The signal around 650 cm^{-1}, which increases slightly in intensity with the increase of the Ca/Si ratio, has been assigned to the Si-O-Si (O-Si-O) bending and water vibrations [90,91].

3.2. Kinetic experiments for the uptake of citrate

3.2.1. AFm phases and ettringite

In a first step the kinetics of citrate uptake on the AFm phases monosulfoaluminate, monocarboaluminate and hemicarboaluminate (Ms, Mc, Hc) and ettringite (AFt) was studied. For the sorption experiments, Ms, Mc, Hc and AFt phases were pre-synthesized and equilibrated for two months before citrate was added to study its sorption. The addition of citrate (at a constant Na concentration of 200 mM) lowered the pH values of AFm phases (from initially ≈13.3) and ettringite (from initially 13.1) by 0.4 pH units, to a pH of 12.9 for Ms and Mc and of 12.7 for ettringite (Fig. 8a). In the case of Hc, the pH was decreased by 0.2 units (from 13.2 to 13.0) only after 1 day, as a consequence of the higher citrate uptake by Hc. The adding of citrate to the suspensions enhanced the dissolution of Ca^{2+} from the solid phase, due to the formation of stable Ca-citrate complexes and/or to the precipitation of Ca-citrate salts (e.g. $Ca_3Cit_2{\cdot}4H_2O$) (Fig. 14).

In general, pH values increased between 1 and 4 days of

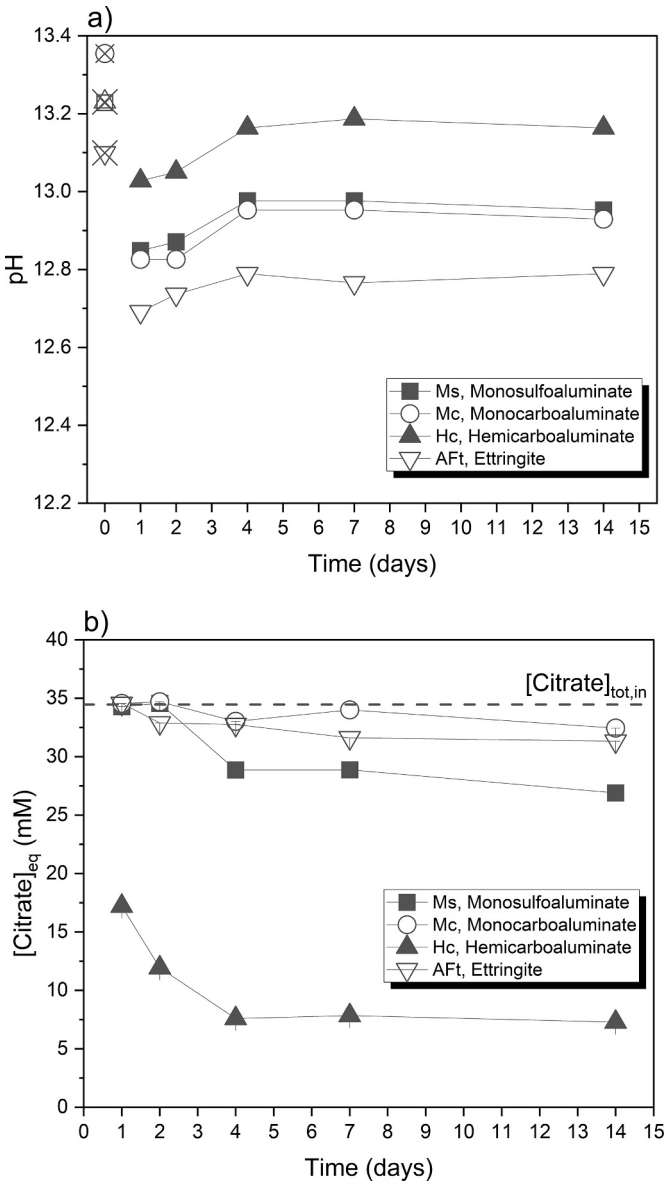

Fig. 8. (a) pH values (measurement error ± 0.1 pH units) and (b) citrate aqueous concentration (measurement error ± 2 %) in the presence of AFm phases (Ms, Mc, and Hc) and AFt measured at different equilibration time (t = 1–14 days) in the presence of initial $[Cit]_{tot}$ = 33 mM and $[Na]_{tot}$ = 0.2 M. Empty crossed symbols indicate the pH values in the absence of citrate.

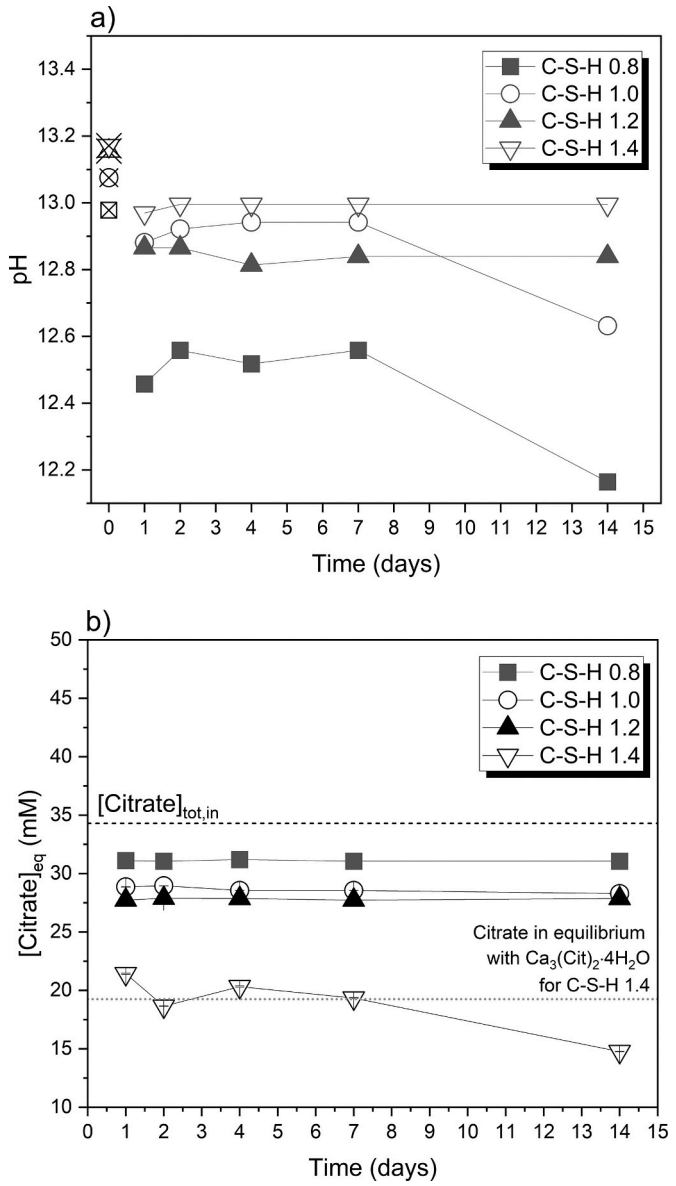

Fig. 9. (a) pH values (measurement error ± 0.1 pH units) and (b) citrate aqueous concentrations (measurement error ± 2 %) in the presence of C-S-H phases (Ca/Si = 0.8–1.4) measured at different equilibration times (t = 1–14 days) in the presence of initial $[Cit]_{tot}$ = 33 mM and $[Na]_{tot}$ = 0.2 M. Empty crossed symbols indicate the pH values in the absence of citrate. The red dotted line represents the citrate concentration in equilibrium with $Ca_3(Cit)_2{\cdot}4H_2O$ at $[Ca]_{tot}$ = 0.025 M representative of the C-S-H 1.4 pore water in 0.2 M NaOH in the absence of citrate.

equilibration, while citrate concentrations decreased up to 4 days (Fig. 8b) significantly in the case of Hc, and moderately for Ms and AFt. For Mc variations of both pH and citrate as function of time were small, indicating a very weak uptake only. In parallel with the changes in pH values and citrate concentrations some variations in aluminium and calcium concentrations were observed during the first 4 days, while they remained stable afterwards (experimental data see Tables S1–S8 in the ESM). Together these data indicate that a steady state sorption was reached within 4 days and little variations occurred between 4 and 14 days. Thus, all further sorption experiments were carried out using an equilibration time of 7 days. In all cases, no additional solids formed due to the addition of citrate (see XRPD data in Figs. S6–S9 in the ESM), although the solution concentration after 1 day indicated oversaturation of the solution with respect to citrate-AFm and citrate-AFt (see Tables S1–S8 in the ESM). However, the formation of these phases was not observed indicating a kinetic hindrance of their formation.

3.2.2. C-S-H phases

Kinetic sorption experiments were also conducted for C-S-H phases. Pure C-S-H phases with a Ca/Si ratio ranging from 0.8 to 1.4 were synthesized as described in the Section 2 and after 2 months of equilibration time, a total citrate concentration of 33 mM was added to the suspension. The addition of citrate decreased the pH by 0.8 pH units for C-S-H 0.8, 0.4 units for C-S-H 1.0, and ≈0.2 units for C-S-H 1.2 and C-S-H 1.4 after 14 days of contacting time (Fig. 9a). The pH values of C-S-H 0.8 and C-S-H 1.0 decreased over time, while the pH values remained constant for Ca/Si = 1.2 and 1.4. In addition, the small amount of portlandite present at Ca/Si = 1.2 and 1.4 was destabilized in the presence of 33 mM citrate, due to the formation of strong $CaCit^-$ aqueous complexes. The XRPD characterization for equilibration time from 1 to 14

days (see Figs. S10–S13 in the ESM), showed that already 1 day after citrate addition portlandite was destabilized.

The measured citrate concentrations were in all cases lower than the initial citrate concentration (Fig. 9b) indicating citrate uptake by C-S-H at all Ca/Si (experimental data see Tables S1–S8 in the ESM). The citrate concentration showed little variation with time, with the exception of C-S-H 1.4, where citrate concentration decreased over time, which is probably related to the slow precipitation of calcium citrate, $(Ca_3(C_6O_5H_7)_2{\cdot}4H_2O$, as observed by XRPD (see Fig. S13 in the ESM). Therefore, a contact time of 7 days was used for further sorption experiments on C-S-H phases as for the sorption experiments on AFm phases and ettringite.

The citrate concentration decreased with the increase of Ca/Si ratio in C-S-H indicating a stronger sorption of citrate in the presence of more calcium. The much lower citrate concentrations measured in the presence of C-S-H with a Ca/Si 1.4, however, are also related to the precipitation of calcium citrate.

3.3. Sorption experiments

3.3.1. Solid AFm phases and ettringite

The composition and structure of Ms and Hc are affected by the presence of citrate (Figs. 10 and 11). The position of the main basal reflection d_{003}, of both Ms12 and Ms14 (monosulfoaluminate with 12 or 14 H_2O moles of water), shifts towards slightly lower degrees 2θ (higher d-values) with the increase of citrate concentration indicating either a very small increase of the interlayer distance due to the intercalation of citrate or more probable, due to a decrease of the number of stacked layers which shifts the XRD signal at a constant basal spacing to lower degrees 2θ values [87,92]. For high citrate concentrations ($[Citrate]_{in}$ = 13 mM and 33 mM) an additional phase was detected with a reflection at 7.2° 2θ (Fig. 10a) corresponding to a d-spacing of 12.2 Å, the position where the basal reflection of citrate-AFm has been observed (see Fig. 2). For Mc no clear effect of citrate on the interlayer distance is observed (Figs. 10 and S14 in the ESM), indicating no significant uptake of citrate in the interlayer of Mc.

In contrast to Mc, the interlayer distances of hemicarboaluminate (Hc) and carbonated hemicarboaluminate (cHc, $C_4Ac_{0.8}H_{10.2}$ [64]) increase clearly with the citrate concentration (Figs. 11b, 12). At the highest citrate concentration (33 mM), only one of the two reflections related to Hc and cHc is present, while at the same time an additional signal at 6.4° 2θ (d-spacing of 13.9 Å) is observed indicating again citrate-AFm or possibly a mixed citrate-carbonate AFm phase (Fig. 11a). The decrease of the intensity of the main basal reflection with the increased citrate concentration may indicate a decrease in ordering and/or more variable interlayer distance. Note that the main layer signal at ≈ 31° 2θ related to the 110 plane did not broaden or decrease in intensity. These findings are in agreement with the observation of the kinetic experiments, where a similar broadening of the basal reflection was observed. A widening of the interlayer due to the intercalation of citrate in the case of Hc, but not for Mc is in agreement with observations of Nedyalkova and co-workers [13]. They detected an anion exchange reaction preferentially on AFm phases with a trigonal structure such as Hc and Ms, but not on Mc, with its rigid triclinic structure and narrow basal spacing.

The effect of citrate on the ettringite structure was also negligible. The pattern of (sulfate-) ettringite is characterized by narrow, well-defined signals. The main (100) signal at 9.1° 2θ (d = 9.7 Å) in *a* direction (perpendicular to the columns) shows only a negligible increase with increasing citrate concentration (Figs. 12 and S14 in the ESM), while for the small (002) reflection (parallel to the column) at 8.2° 2θ (d = 10.7 Å) no significant variations are observed.

The uptake of citrate in Ms and Hc is also well visible in the FTIR spectra (Fig. 13), where the intensities of the stretching vibration band of the citrate carboxylate group are growing, while the vibration bands of the sulfate group decreases with increasing citrate concentrations. The increase of the signal of the carboxylate group of citrate is much more intense for Hc than for Ms, indicating a more intense uptake of citrate in agreement with XRPD results.

In the case of Mc, the bending vibrations of CO_3^{2-} (1450–1400 cm^{-1}, see Fig. S16 in the ESM) slightly decrease with the increase of citrate concentration, indicating a low tendency of citrate sorption via anion exchange reaction than for Ms and Hc.

In the case of ettringite the stretching vibrations of carboxylate group of citrate are covered by the bending vibrations of Ca = OH_2 (1660 cm^{-1}) [84], while the intensity of the sulfate stretching vibration at ≈1100 cm^{-1} shows some variations (see Fig. S17 in the ESM), but no systematic decrease with citrate concentration indicating no or only very little replacement of sulfate by citrate. This finding is also in agreement with the XRPD characterization, where no significant changes in the ettringite structure were found in the presence of citrate.

3.3.2. Aqueous concentrations in equilibrium with AFm phases and ettringite

All measured data and calculated saturation indices are provided in Tables S17–S24 in the ESM. Fig. 14 shows that the addition of citrate increases the calcium and sulfate concentrations but lowers the pH values in the presence of AFm phases and ettringite. The increase of the

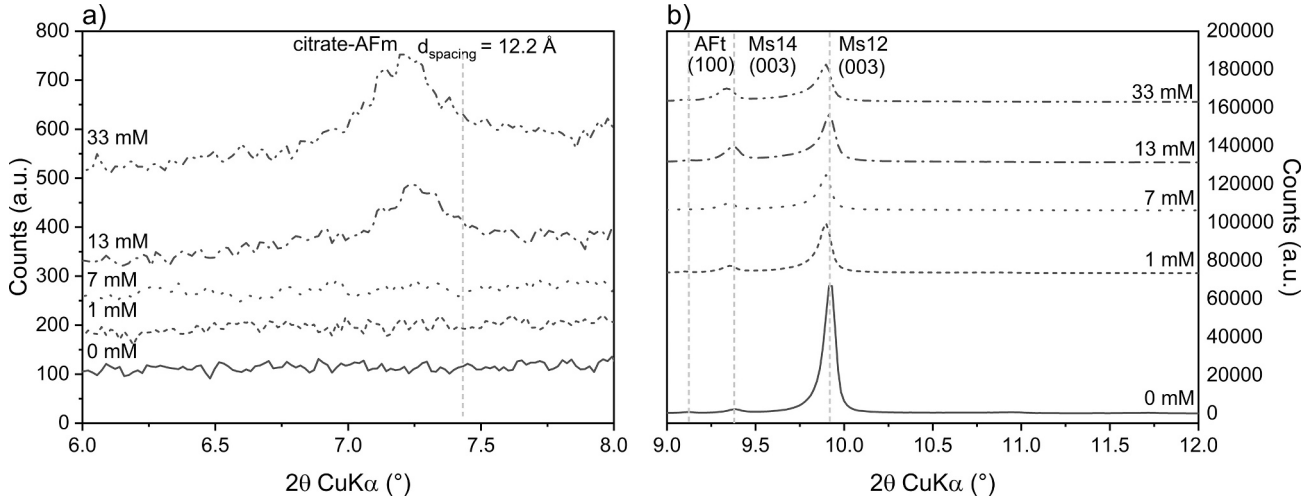

Fig. 10. XRPD patterns of monosulfoaluminate after sorption of citrate and for contacting time t = 7 days. (a) Appearance of citrate-AFm at higher dosages of citrate, and (b) Shift of basal spacing of Ms, monosulfoaluminate (Ms12 and Ms14 indicates the water content of monosulfoaluminate).

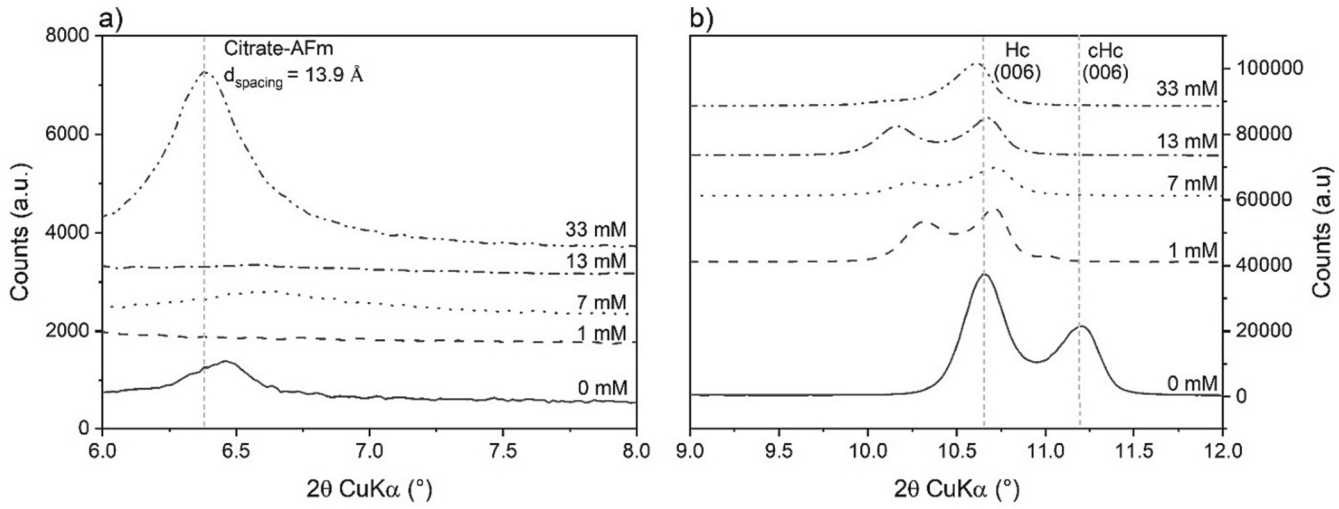

Fig. 11. XRPD patterns of hemicarboaluminate after sorption of citrate and for contacting time t = 7 days. (a) Appearance of citrate-AFm at higher dosages of citrate and (b) Shift of basal spacing of Hc, hemicarboaluminate.

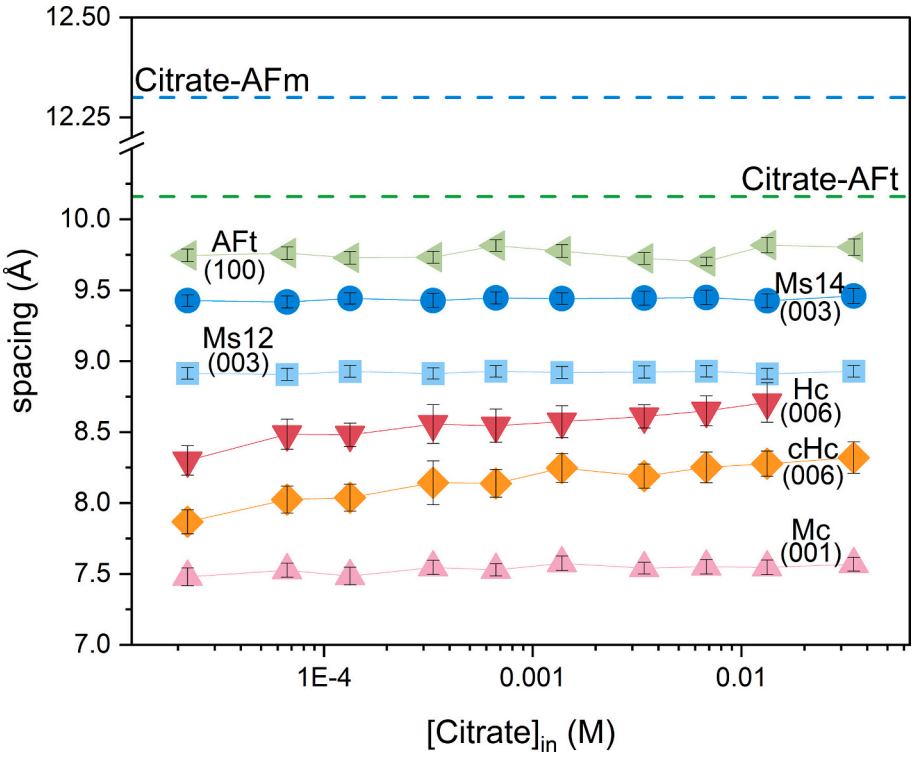

Fig. 12. Increase of the basal spacing (00x) for AFm phases (for comparison: basal spacing of citrate-AFm = 12.3 Å) and the a-spacing (x00, perpendicular to the columns) of sulfate ettringite (AFt) (for comparison: interplanar distance of citrate-AFt = 10.2 Å) in the presence of citrate.

sulfate concentration for Ms and ettringite in the presence of citrate indicates a partial replacement of sulfate by citrate. The increase of the calcium concentration with citrate addition is mainly due to the formation of aqueous $CaCit^-$ complexes, which dominate Ca speciation at citrate concentrations at >1 mM as exemplified for Mc in Fig. 15. $CaCit^-$ has been found the most stable aqueous Ca complex in the presence of 2 mM citrate and above in the presence of all AFm phases and ettringite studied here. Citrate is present in solution mainly as fully deprotonated Cit^{3-} species. At high calcium concentrations and low citrate concentrations a significant fraction $CaCit^-$ is calculated to form, while the fraction of citrate complexes with Na, K or Al were negligible (<0.1 % of citrate) under all conditions considered. Although ettringite samples have the lowest Ca concentration at low citrate concentrations, the Ca concentrations increase steeply and reach comparable calcium concentrations at high citrate concentrations as observed for the AFm phases. In the case of Hc and AFt, however, the Ca concentrations drop at the highest citrate concentrations, where the solutions are oversaturated with respect to Ca-citrate ($Ca_3(Cit)_2{\cdot}4H_2O_{(s)}$), as detailed in Table S22 (hemicarboaluminate) and S24 (ettringite) in the ESM, pointing towards the possible precipitation of Ca-citrate. The saturation indices calculated from the measured aqueous concentrations showed also a strong oversaturation with respect to citrate-AFm and citrate-AFt indicating a kinetic hindrance of their formation in the sorption experiments conducted.

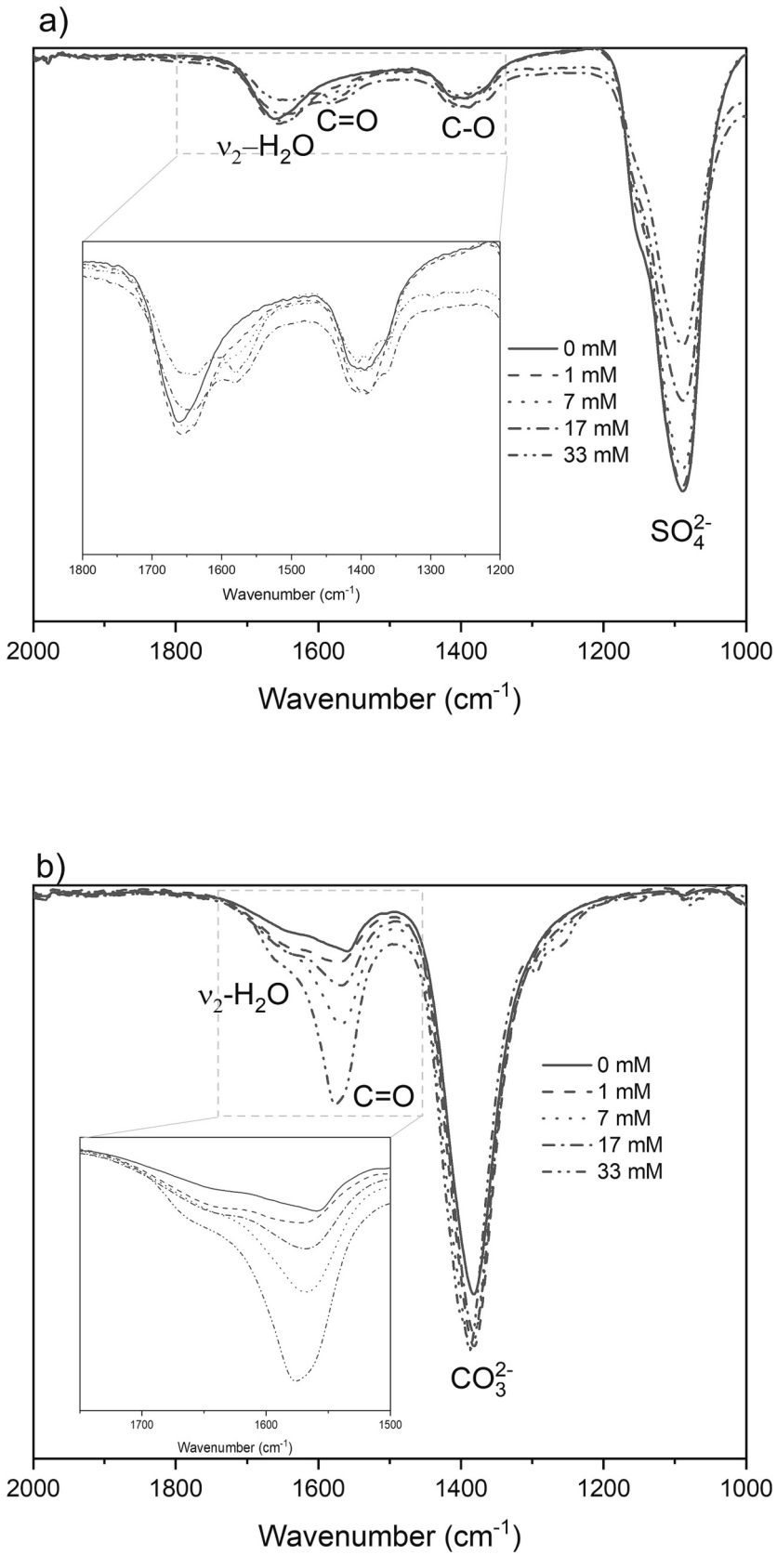

Fig. 13. Effect of the initial citrate concentration on the FTIR spectra of (a) Ms, monosulfoaluminate and (b), Hc, hemicarboaluminate at 7 days of contacting time after the citrate adding.

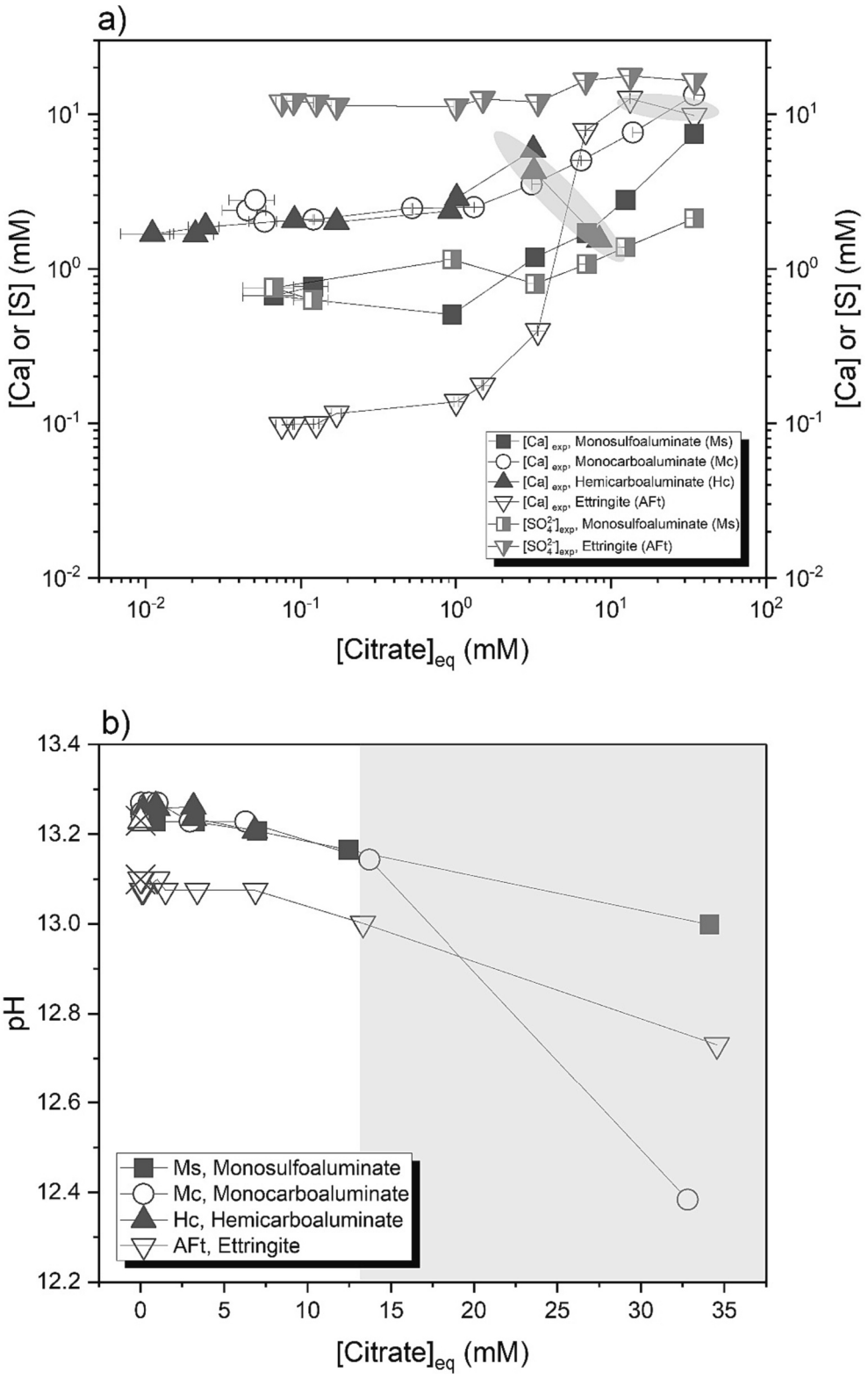

Fig. 14. (a) Measured Ca aqueous concentration and (b) pH values of AFm phases (Ms, Mc, and Hc) and AFt, with $[Na]_{tot} = 0.2$ M and a contacting time of 7 days. Shaded grey areas indicate the regions where Ca-citrate formation is expected based on SI calculation.

The sorption of citrate on AFm phases and ettringite is shown in Fig. 16. The overall sorption capacity of AFm phases refers to the sum of surface sorption sites and interlayer sorption capacity. Assuming that the main sorption uptake mechanism occurs via electrostatic interaction between the positive charged layer and the accommodating anion, the total molar capacity per kg of solid for citrate is based on the valence of citrate in the anionic form (−3) and the total positive charge (+2) of the main layer $Ca_4Al_2(OH)_{12}^{2+}$ per formula unit. The batch experiments, carried out at pH ≈ 13, show that citrate sorbs at low concentrations significantly on Hc and on Ms, while the uptake on Mc and AFt is rather weak. The citrate sorption on Mc, Ms and ettringite increases with citrate concentration up to ≈ 0.01 mol citrate per kg solid, while little

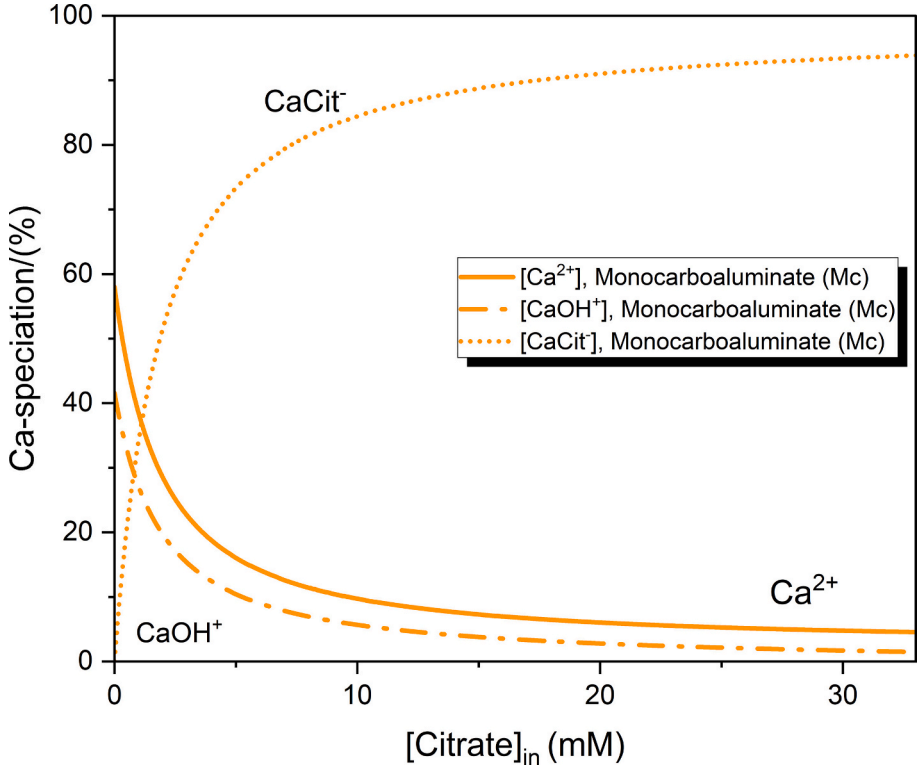

Fig. 15. Calculated fraction of Ca-complexes in the equilibrium with Mc as a function of added citrate concentration.

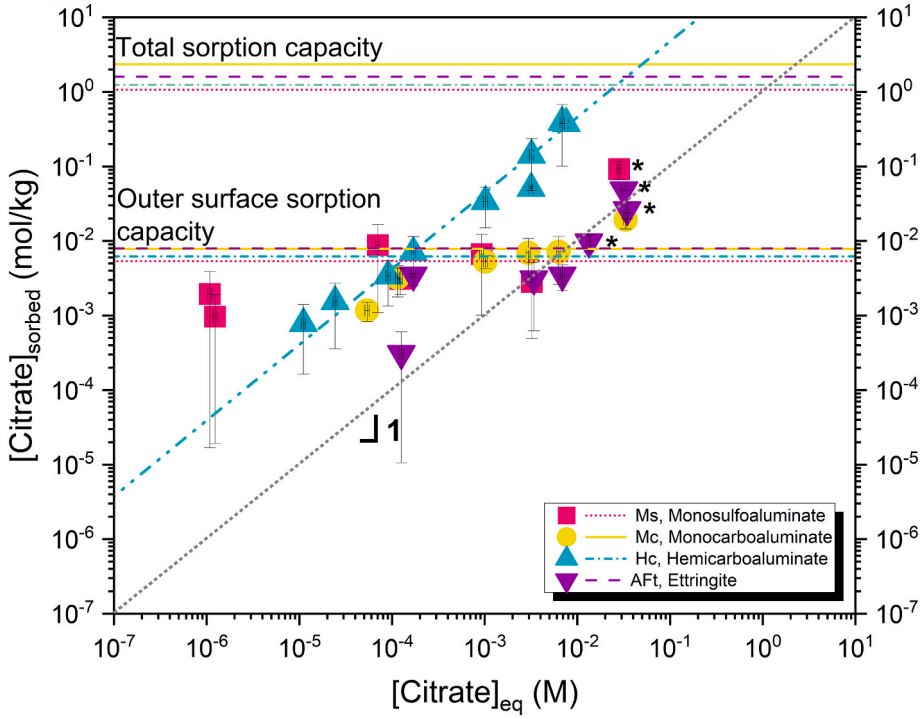

Fig. 16. Experimental citrate sorption isotherm for monosulfoaluminate (Ms), monocarboaluminate (Mc), hemicarboaluminate (Hc) and ettringite (AFt) after an equilibration time of 7 days. The upper and lower horizontal lines indicate the total potential total surface uptake potential uptake on the outer surface of Ms, Mc, Hc and AFt respectively. Symbols marked with (*) indicate the potential precipitation of $Ca_3Cit_2{\cdot}4H_2O$ based on the calculated saturation indices in ESM Section 3.

additional sorption is observed at higher citrate concentrations. Above 6 mM citrate, the formation of Ca-citrate ($Ca_3(Cit)_2{\cdot}4H_2O_{(s)}$) is expected for ettringite as indicated by the star symbol in Fig. 16. The total possible uptake of citrate on Ms, Hc, Mc and ettringite corresponds to ≈1 mol per kg solid as indicated by the horizontal lines in Fig. 16. The limited sorption of ≈0.005 mol citrate per kg Ms, ettringite and Mc might be related to a limitation of the citrate sorption to the outer surface only. Ma et al. and Nedyalkova et al. [15,93] reported a ratio of outer to total

surface sites for AFm phases of 1:1000 and 1:60 respectively. Nedyalkova et al. [93] observed in the case of Mc that also iodide ions sorption occurred on the outer surface only. Based on the observed limited uptake observed for citrate it can be expected that citrate sorbs in the case of Mc, Ms and ettringite on the outer surface mainly and that the ratio of outer surface sites to total (outer and interlayer) surface sites corresponds to 1:200, as indicated by the horizontal lines labelled as outer surface sorption capacity in Fig. 16.

Only in the case of Hc, sorption increases with citrate concentration with a slope of 1, indicating a high affinity of citrate to sorb on Hc. The quasi-linear trend of Hc for 10^{-5} M < $[Citrate]_{eq}$ < 1 M Hc suggests that both the inner and outer surface sites of Hc can be occupied by citrate. The higher sorption capacity can be related to the weak linkage energy (hydrogen bonds) of the interlayer anion OH^- present in the case of Hc as well as to its larger basal spacing, which makes the uptake of citrate easier.

For Ms also a strong uptake is observed at low citrate concentrations, but only up to ≈ 0.005 mol/kg Ms, indicating that only outer surface sites of Ms can be occupied by citrate. This observation is also in agreement with the strong decrease of the zeta potential of Ms up to ≈0.01 mol/kg Ms (see Fig. S18 in ESM), which continued more moderately for citrate concentration up to ≈3 mM, confirming a strong sorption of citrate on the outer surface of Ms. The liquid phase analyses evidenced no significant increase of the sulfate concentrations at low citrate concentrations with a more or less constant sulfate concentration of 1 mM. A moderate increase was observed at citrate concentrations of ≥6.7 mM, where the pH started to be lowered. This underlines a very limited uptake of citrate in monosulfoaluminate being in contrast with the observations for smaller anions such as I^-, where a continuous and complete replacement of sulfate by iodide in monosulfoaluminate was observed by Aimoz and Nedyalkova [13,94].

For AFm phases, R_d values of ≈10 (Mc), ≈40 (Hc) and ≈230 L/kg (Ms) were derived for citrate concentrations <0.1 mM, while the R_d of ettringite was in the range of 1 to 18 L/kg. At higher citrate concentrations these values decreased strongly by about ≈2 order of magnitude (Mc, Ms and AFt) due to limited accessibility of citrate to the available sorption sites.

3.3.3. Solid C-S-H phases

Fig. 17 compares the XRPD patterns of C-S-H in the presence of 33 mM citrate with C-S-H samples without citrate. As described previously [46,86] (Section 3.1.3), the d-spacing of C-S-H phases decreases with increasing Ca/Si ratio. Detailed studies indicate that this reduction of interlayer distance could be related to the strong attracting effect of the Ca^{2+} in the interlayer towards the negatively charged main layer [25]. The presence of citrate has a negligible effect on the basal spacing of low Ca/Si (0.8 and 1.0) C-S-H phases, while a more accentuated decrease of the basal spacing from 12.2 to 10.8 Å at Ca/Si = 1.2 and from 11.3 Å to 9.7 Å at Ca/Si = 1.4 are visible on the shift of the 002 band towards higher diffraction angles. Such a decrease of the interlayer distance has been reported previously at lower pH values and higher Ca-concentrations [86] as the presence of more Ca^{2+} in the interlayer resulting in a stronger attraction between the two main layers. However, this is not the case here, as less Ca in C-S-H is observed in the presence of higher citrate concentrations (see below), thus the decreased layer distance could possibly be due to a decreased repulsion between the main C-S-H layer at increased ionic strength in the presence of high citrate concentrations. A slight decrease of Ca/Si ratio in the C-S-H is observed for citrate concentration higher than 0.003 M (see Fig. S19 in the ESM), due to the presence of more dissolved Ca and the formation and

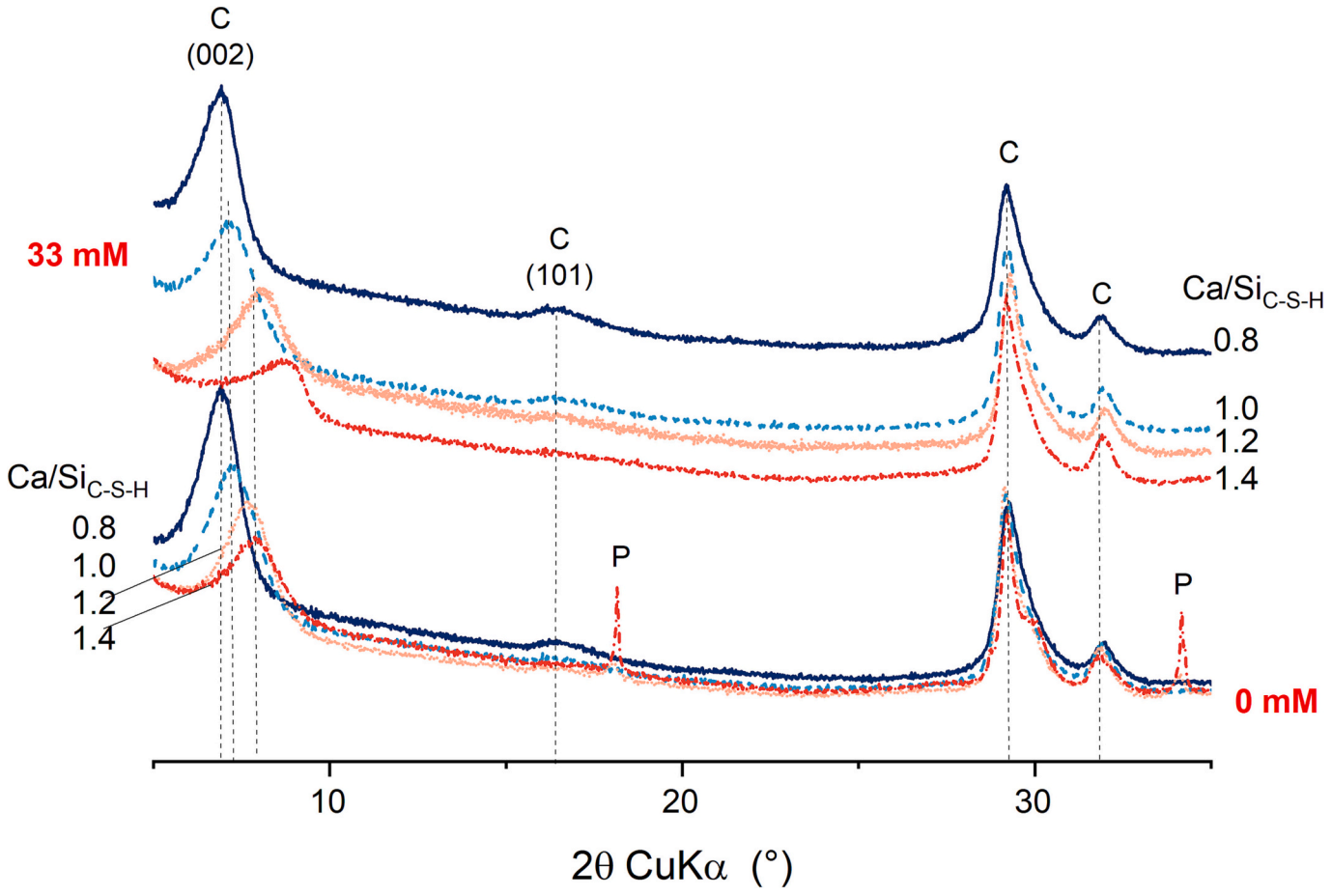

Fig. 17. XRPD characterization of C-S-H phases (Ca/Si = 0.8–1.4) in presence (33 mM) and in absence of citrate after 7 days of contacting time after citrate addition.

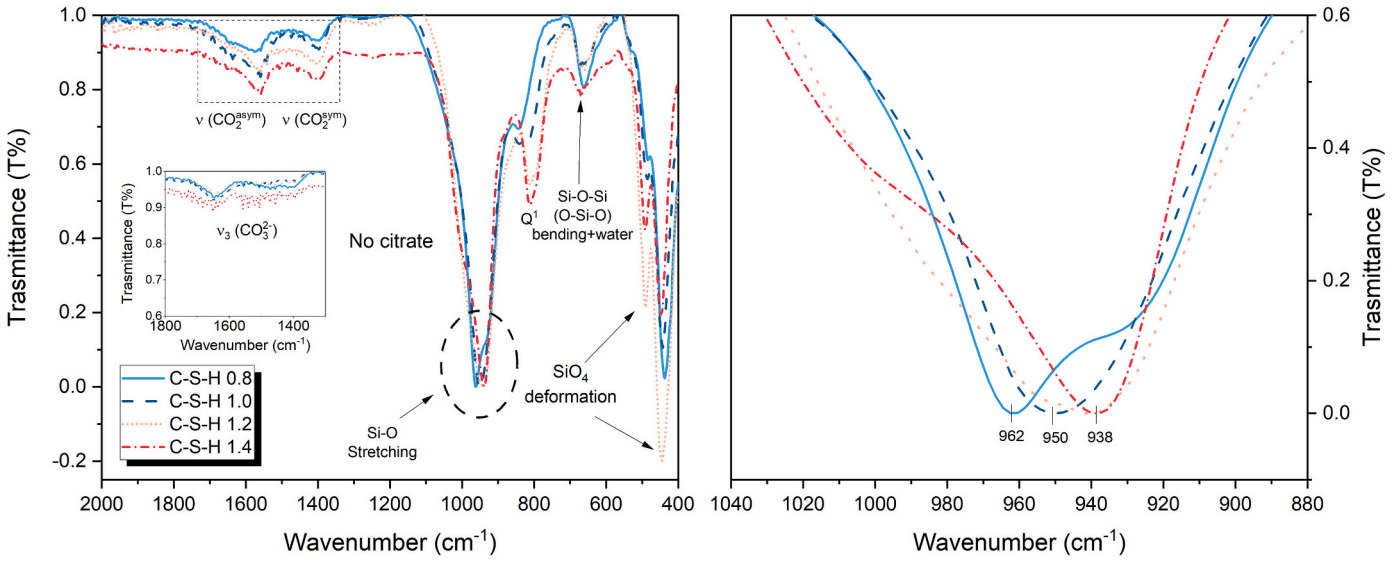

Fig. 18. FTIR characterization of C-S-H phases (Ca/Si = 0.8–1.4) equilibrated with 33 mM citrate for 7 days of contacting time in the wavenumber region 2000–400 cm^{-1}.

precipitation of $Ca_3Cit_2{\cdot}4H_2O$, as also suggested by the calculated saturation indices (see Tables S9–S16 in the ESM).

In addition, the small amount of portlandite originally present at Ca/Si = 1.2 and 1.4, is destabilized in the presence of 33 mM citrate for Ca/Si = 1.2 and 7 mM citrate for Ca/Si = 1.4, due to the formation of $CaCit^-$ aqueous complexes (Fig. 15).

The FTIR of C-S-H phases (Ca/Si = 0.8–1.4) equilibrated for 7 days with 33 mM citrate in Fig. 18 shows the typical stretching band of the Si—O bond at ≈950 cm^{-1}, which shifts systematically towards lower wavenumbers with higher Ca/Si as also observed in the absence of citrate (Fig. 7). The presence of citrate led to somewhat higher wavenumbers in particular for the low Ca/Si C-S-H samples. The Q^1 band at 840–810 cm^{-1} increases in intensity and shifts towards lower wavenumbers with the increase of the Ca/Si ratio. The comparison with the citrate-free C-S-H samples indicates less Q^1 sites in the presence of citrate and thus less Ca in C-S-H, in particular for Ca/Si = 1. This is consistent with the increased Ca-fraction observed in the solution, as discussed in the next section. In the presence of citrate, additional bands occurred in the wavenumber region of 1550 and at 1400 cm^{-1} indicating the presence of citrate in C-S-H for all Ca/Si ratios, as also observed for the AFm phases in Fig. 3b.

3.3.4. *Aqueous concentrations in equilibrium with C-S-H phases*

All measured data and calculated saturation indices are provided in Tables S25–S32 in the ESM. The total Ca concentration in solution and the pH values as a function of the citrate concentration are shown in Fig. 19. The Ca concentration (Fig. 19a) increases for all C-S-H phases with increase of citrate concentration. For low citrate concentrations ($[Citrate]_{eq}$ < ≈0.1 mM), no significant effect on the calcium concentrations is observed, while for 1 mM citrate and above the calcium concentrations are increased due to the formation of aqueous $CaCit^-$ complexes as observed above for the AFm phases and ettringite. In addition, as mentioned in Section 3.3.3, citrate affects the C-S-H phase composition by dissolving more Ca^{2+} with increasing citrate concentration and therefore lowering the Ca/Si in the solid in agreement with the presence of less Q^1 sites and thus lower Ca/Si ratios observed by FTIR. The total Ca concentrations reach 6 to 17 mM at 30 mM citrate, depending on the Ca/Si ratio of the initial C-S-H. Fig. 19b illustrates the decrease of pH with increasing addition of Na_3-citrate, in particular for low Ca/Si C-S-H, which is able to bind significant amounts of Na^+ in its ion exchanges sites [86]. The effect is much smaller at higher Ca/Si, where less Na^+, but rather citrate is bound within the structure. The addition of citrate lowers the pH significantly as the major fraction of the citrate remains in solution, in particular in the presence of low Ca/Si C-S-H.

The sorption of citrate at pH of ≈13.2 on C-S-H is expressed in Fig. 20 as moles of citrate adsorbed per kg of C-S-H. The weight of C-S-H has been determined by combining mass balance calculations and water content obtained by TGA analysis as detailed in Electronic Supplementary Materials (Table S33). Fig. 20 shows a clear increase of citrate sorption with the Ca/Si ratio or also with the calcium concentration in solution (Fig. 19). Similar observations have been reported for gluconate sorption on C-S-H and portlandite, where the gluconate uptake is mediated by the presence of Ca^{2+} at the surface [20,95]. A comparable mediation of citrate uptake on C-S-H by Ca^{2+} can thus be expected.

For citrate concentration higher than 2 mM, where the formation of $CaCit^-$ complexes dominates the solution composition (see also Fig. 15), the sorption of citrate on C-S-H levels off or even decreases by one order of magnitude (based on the steepness of the sorption isotherm eye-guide line shown in the Fig. 20) at Ca/Si = 0.8, where little calcium is available. This decrease of the sorption at higher organic anion concentrations has also been observed for gluconate [95], where the formation of aqueous calcium gluconate complexes led to a desorption of Ca^{2+} from the solid C-S-H surface up to a point, where no sufficient Ca^{2+} was available at the surface to mediate gluconate or citrate (as in this study) sorption. Such a behavior was predicted by Turesson and coworkers [96] based on Monte-Carlo simulations for the Ca^{2+} mediated adsorption of polyanions on negatively charged surfaces.

For the C-S-H phases, R_d values of (3.0 ± 1.3) $L{\cdot}kg^{-1}$, (16.6 ± 2.2) $L{\cdot}kg^{-1}$, (39.5 ± 3.8) $L{\cdot}kg^{-1}$ and (52.6 ± 4.7) $L{\cdot}kg^{-1}$ were derived at citrate concentrations <2 mM for Ca/Si = 0.8, 1.0, 1.2 and 1.4 respectively. For high citrate concentrations, the amount of citrate sorbed on C-S-H Ca/Si = 1.2 and 1.4 in Fig. 19 did not increase anymore due to the desorption of Ca^{2+} from the C-S-H surface as illustrated in Fig. 19a.

Previous studies have shown that the uptake of cations [97,98] or anions [48,99,100] on C-S-H can increase or decrease the charge near the Stern layer determined by zeta potential measurements. Zeta potential measurements carried out on C-S-H containing suspensions in the presence of citrate are shown in the Fig. 21. The zeta potential in the absence of citrate is negative for C-S-H with a Ca/Si = 0.8 due to the deprotonation of ≡Si-OH surface groups to ≡Si-O^- at pH values above 10. The higher the pH, the higher the negative charge of low Ca/Si C-S-H [29,101,102]. The sorption of Ca^{2+} on the surface of C-S-H: ≡Si-OCa^+, can compensate or even overcompensate this negative charge leading to

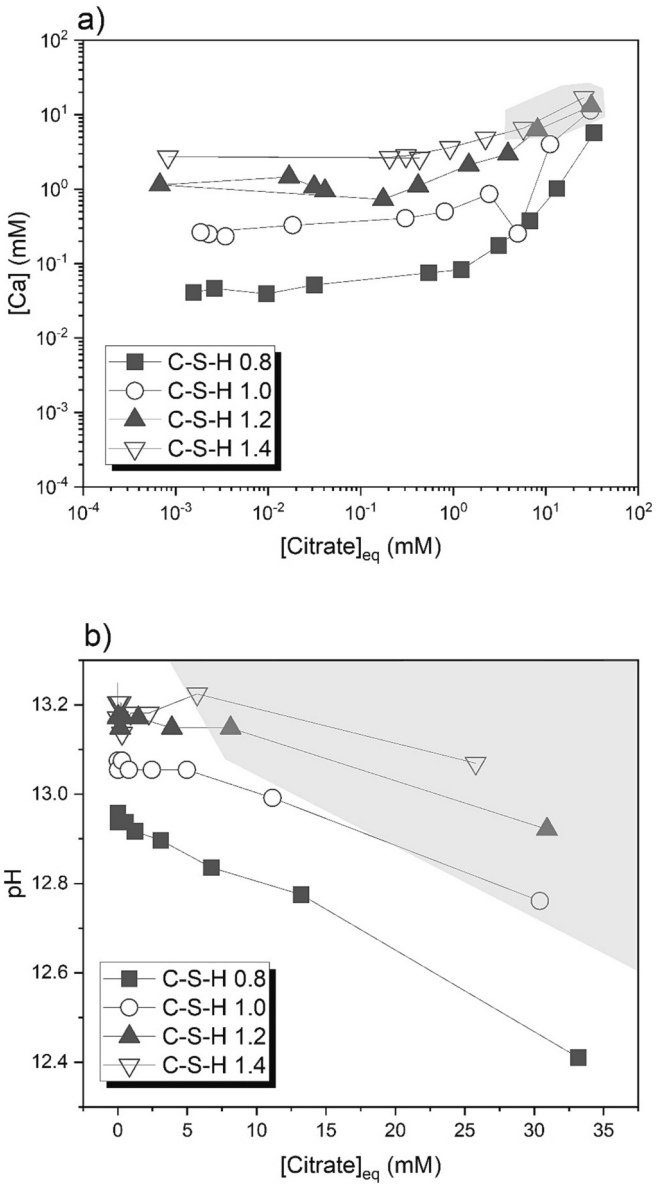

Fig. 19. (a) [Ca] aqueous concentration and (b) pH values for C-S-H phases (Ca/Si = 0.8–1.4) as function of citrate concentration in solution measured after 7 days of contacting time. Shaded grey areas indicate the regions where Ca-citrate formation is probably based on SI calculation.

positive zeta potential measurements at high calcium concentrations [103,104], see left side of Fig. 21. Fig. 21 shows also that the addition of citrate decreases the zeta potential of the C-S-H phases as well as the one of portlandite, indicating an accumulation of citrate at the surface, leading to the observed charge reversal, similarly as observed by Nachbaur et al. [97] for sulfate on the C-S-H surface. The amount of citrate needed to reach the isoelectric point increases with the increase of Ca/Si ratio. For Ca/Si = 0.8 already the initial zeta potential is negative and little further change is observed above 0.04 mol citrate per kg of solid (~ 2 mM citrate). For Ca/Si = 1.0, 1.2 and 1.4 the charge is reversed at 0.02 mol citrate per kg of solid (~1 mM citrate), 0.04 (~2 mM) and 0.08 (~4 mM), respectively. Also on PC, a decrease of the zeta potential was observed [105] in the presence of 2 wt% of Na_3-citrate and K_3-citrate. The zeta potential of portlandite reported as reference system in Fig. 21, presents a similar decreasing trend with increasing citrate addition, and a negative charge is observed for high citrate concentrations. The formation of negative surface charge (negative zeta potential) in the presence of citrate is consistent with the observed citrate sorption on C-S-H in Fig. 20.

3.3.5. *Sorption of citrate on hydrated cement*

In Fig. 22 the R_d coefficients obtained in this study for the different cement phases, monosulfoaluminate, monocarboaluminate, hemicarboaluminate, ettringite and C-S-H phases with Ca/Si ratio ranging from 0.8 to 1.4 are reported as a function of equilibrium calcium concentrations based on the R_d values obtained at citrate equilibrium concentration below than 2 mM, i.e. at conditions where sorption is the main process, and Ca-citrate precipitation can be excluded. Citrate sorbs most strongly on Ms and Hc, followed by Mc and ettringite. It is evident that citrate has a higher affinity to the layered structure of AFm phases than to the hexagonal ettringite. As discussed in the Section 3.3.1, citrate sorption occurs mainly on the outer surface of Ms, Mc and ettringite which strongly limits the maximum uptake, while citrate seems to be able to enter also the interlayer region in the case of Hc. Citrate sorption on C-S-H phases is generally weaker but increases with the Ca/Si ratio, indicating that Ca^{2+} mediates citrate sorption. Only a few studies investigated the uptake of citrate on hydrated cements. Möschner et al. [3] investigated the uptake of citric acid (at initial citrate concentration of 13 mM, 52 mM and 65 mM) on a Portland cement (PC). The R_d coefficient shown in the Fig. 22 corresponds to the initial citrate content of 65 mM after 28 days. The citrate sorption on PC is with R_d value of 12.5 $L{\cdot}kg^{-1}$ comparable to the R_d values of C-S-H with a Ca/Si ratio of 1.4, monocarboaluminate and ettringite, the main hydrates observed in addition to portlandite in the hydrated PC [3]. In the present study an even higher R_d of (154 ± 20) $L{\cdot}kg^{-1}$ was observed for PC, which might be related to the presence of more AFm phases (i.e. hemicarboaluminate and monocarboaluminate) in the cement studied here (see Figs. S20 and S21 in the ESM), compared to [3] where no significant amount of AFm phases was reported due to the higher SO_3 to Al_2O_3 ratio in the cement used by [3]. Another relevant factor is the higher pH values present in the pore solution of the hydrated cement (pH ≈ 13.7), [3]), than in the sorption experiments conducted in the title study at a pH of ≈13.3. High pH values lead to a more negative surface charge of the hydrates [48], lower calcium concentrations and therefore a lower sorption of citrate on PC in the study of [3] than measured in the present study. Even though [3] observed a R_d value of only ≈13 $L{\cdot}kg^{-1}$ < 2 % of the initial citrate was observed in the cement pore solution after longer equilibration times, while >98 % of the initial citrate were sorbed on solid phases [3].

As C-S-H is the major phase in hydrated Portland and blended cements, the composition of C-S-H plays an important role for citrate sorption, and citrate sorption is expected to be lower in the presence of Si-rich supplementary cement material (SCMs) where C-S-H with a lower Ca/Si is formed than in Portland cements [106,107]. The R_d value calculated for a calcium aluminate (CA) cement hydrated for 10 min [108] is much lower, which is related to the absence of C-S-H or AFm phases in CA cements, where mainly katoite ($Ca_3Al_2(OH)_{12}$) and Al $(OH)_3$ are formed, which seem to show little affinity for citrate.

4. Conclusion

The sorption of the citrate $(C_6H_5O_7)^{3-}$ on the main hydrates formed in Portland and blended cements has been investigated at a pH of ≈13.2. Citrate sorption on monosulfoaluminate, monocarboaluminate, hemicarboaluminate (AFm phases), ettringite and C-S-H phases was determined. For comparison, also "pure" citrate-AFm and citrate-AFt were synthesized, which exhibit a relatively poorly-ordered structure. For citrate-AFm a basal spacing of 12.2 Å has been observed, comparable to the value reported by Pöllman and co-authors [66] and comparable to the values observed for citrate-containing LDH phases. The uptake of citrate in the ettringite structure increased the distance along the a-axis (x00, perpendicular to the columns) from 9.7 Å for the sulfate based ettringite to 10.2 Å for citrate-AFt. Citrate-AFm and citrate-AFt were

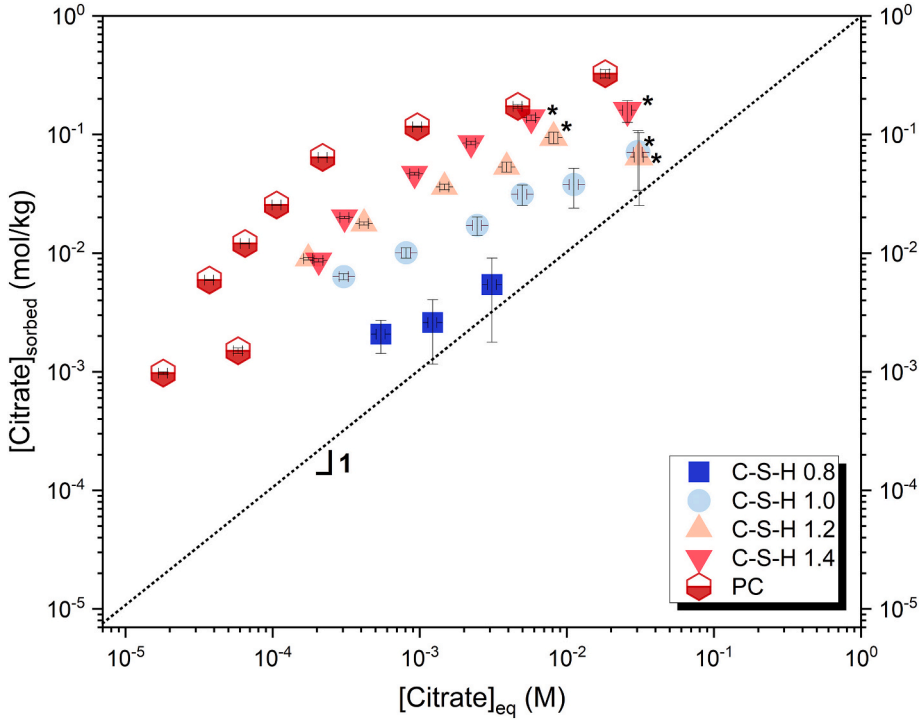

Fig. 20. Sorption isotherms calculated as moles of citrate sorbed per kg of solid phase, for C-S-H phases with a ratio of 0.8 ≤ Ca/Si ≤ 1.4 and Portland cement (PC) after 7 days of contacting time the citrate adding. Symbols marked with (*) indicated the possible formation of $Ca_3Cit_2{\cdot}4H_2O$ as suggested by the calculated saturation indices.

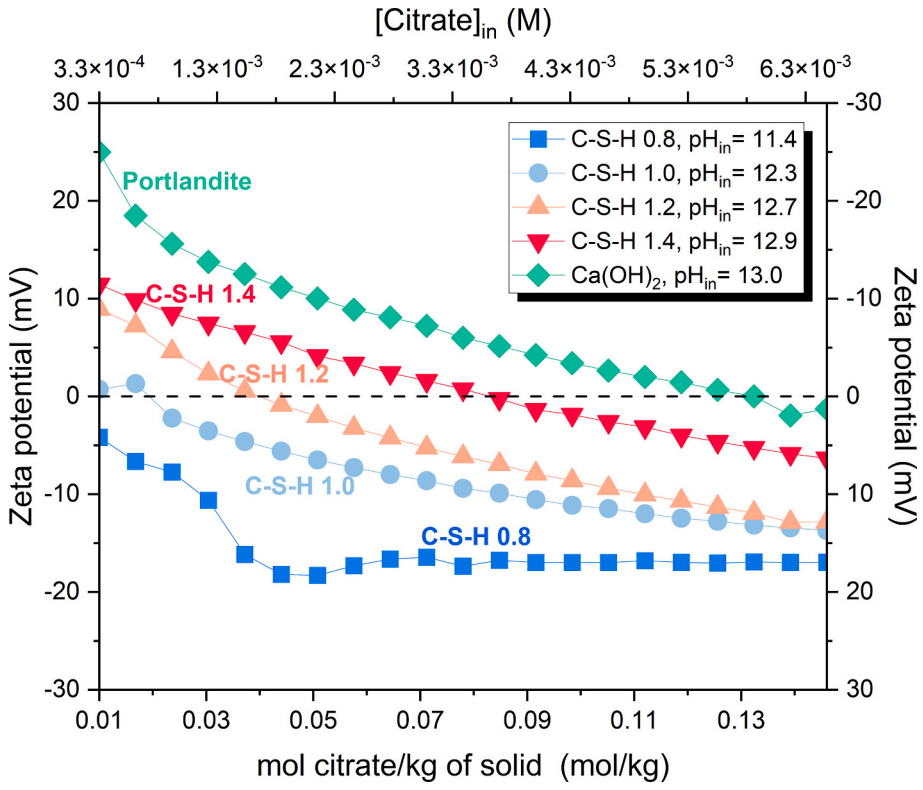

Fig. 21. Zeta potential measured in the presence of citrate in C-S-H suspensions with a Ca/Si ratio of 0.8, 1.0, 1.2 and 1.4 and portlandite suspensions.

found to be less stable than sulfate- or carbonate-containing AFm phases and ettringite, respectively.

Kinetic sorption experiments of citrate on pre-synthesized monosulfoaluminate, monocarboaluminate, hemicarboaluminate, ettringite and C-S-H phases indicated a relatively fast uptake of citrate; steady-state sorption was attained within 4 days. The sorption experiments at $[Citrate]_{in} = 10^{-5}$ M to 10^{-1} M indicated that citrate tends to sorbs mainly on outer surface sites of monosulfoaluminate,

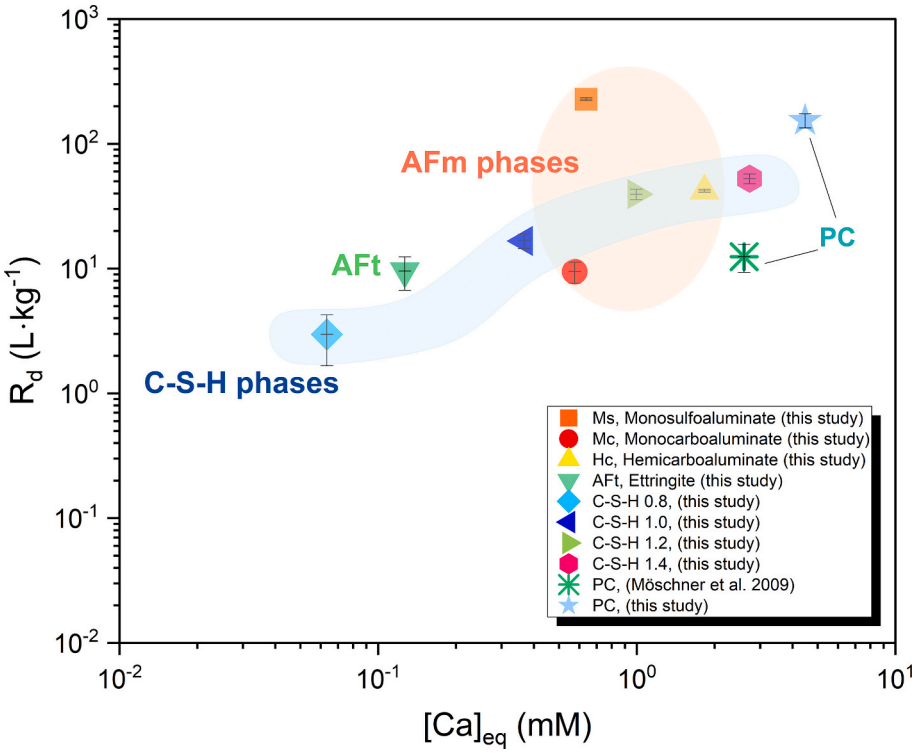

Fig. 22. Comparison of R_d coefficients for citrate sorption on AFm phases, ettringite and C-S-H phases with Ca/Si = 0.8, 1.0, 1.2 and 1.4, for citrate concentration < 2 mM, with R_d observed for hydrated Portland cement, PC, by Möschner et al. [3] and in this study.

monocarboaluminate and ettringite, while the formation of citrate-AFm and citrate-AFt was kinetically hindered. Only for hemicarboaluminate, which has a larger basal spacing, sorption occurred both in the interlayer and surface sorption sites resulting in much larger sorption capacity of hemicarboaluminate compared to monosulfoaluminate or monocarboaluminate. The formation of $CaCit^-$ complexes led in all cases to a strong increase of total calcium concentrations in solution observed in all experiments upon the addition of citrate.

The sorption of citrate on C-S-H increased with the Ca/Si ratio and with the calcium concentration in solution, similar to observations for gluconate uptake on C-S-H and portlandite, which is mediated by the presence of Ca^{2+} at the surface. Below 2 mM of citrate a more or less linear increase of citrate sorption on C-S-H phases was observed, while at higher citrate concentrations, where formation of aqueous $CaCit^-$ complexes led to a desorption of Ca^{2+} from the solid C-S-H, the sorption of citrate on C-S-H leveled off or even decreased. The sorption of citrate on C-S-H (and portlandite) was also evidenced by the strong decrease of the surface charge observed in the presence of citrate by zeta potential measurements.

The partitioning of citrate between solid and liquid phase is described in terms of R_d factors. Citrate sorbed most strongly on hemicarboaluminate and monosulfoaluminate, followed by monocarboaluminate and ettringite. The sorption on C-S-H with a high Ca/Si is comparable to Hc, while the citrate sorption decreased strongly for C-S-H with lower Ca/Si. The sorption coefficients of citrate measured on hydrated Portland cement were with R_d = 10–200 L·kg^{-1} comparable to the sorption observed on high Ca/Si C-S-H ($R_d \approx 50$ L·kg^{-1}) and AFm phases (R_d = 10–200 L·kg^{-1}) indicating a strong uptake of citrate in hydrated cements. A higher citrate uptake was observed for a PC rich in AFm phases (monocarboaluminate and hemicarboaluminate) at pH of 13.3 than for a PC with no or only little AFm phases at a pH of 13.7. Citrate sorption is expected to be higher at lower pH values and higher calcium concentrations. These results also emphasize that the availability of citrate for the complexation of radionuclides in the context of repositories for L/ILW will be significantly decreased through the uptake by cementitious materials.

CRediT authorship contribution statement

Rosa Ester Guidone: Methodology, Investigation, Validation, Writing – original draft, Writing – review & editing. **Xavier Gaona:** Conceptualization, Writing – review & editing, Supervision. **Frank Winnefeld:** Writing – review & editing, Investigation. **Marcus Altmaier:** Writing – review & editing, Project administration, Funding acquisition. **Horst Geckeis:** Writing – review & editing, Supervision. **Barbara Lothenbach:** Methodology, Validation, Conceptualization, Writing – review & editing, Supervision.

Declaration of competing interest

The authors declare that they have no known competing financial interests or personal relationships that could have appeared to influence the work reported in this paper.

Data availability

Data will be made available on request.

Acknowledgments

The support of L. Brunetti and B. Ingold during the laboratory work is gratefully acknowledged. The EURAD project leading to this application has received funding from the European Union's Horizon 2020 research and innovation programme under grant agreement No 847593.

Appendix A. Supplementary data

Supplementary data to this article can be found online at https://doi.org/10.1016/j.cemconres.2023.107404.

References

[1] N. Wang, H. Yu, W. Bi, Y. Tan, N. Zhang, C. Wu, H. Ma, S. Hua, Effects of sodium citrate and citric acid on the properties of magnesium oxysulfate cement, Construct. Build Mater. 169 (2018) 697–704.

[2] I. Oliveira, F. Ortega, V. Pandolfelli, Hydration of CAC cement in a castable refractory matrix containing processing additives, Ceram. Int. 35 (2009) 1545–1552.

[3] G. Möschner, B. Lothenbach, R. Figi, R. Kretzschmar, Influence of citric acid on the hydration of Portland cement, Cem. Concr. Res. 39 (2009) 275–282.

[4] A. Kusbiantoro, M.S. Ibrahim, K. Muthusamy, A. Alias, Development of sucrose and citric acid as the natural based admixture for fly ash based geopolymer, Procedia Environ. Sci. 17 (2013) 596–602.

[5] N. Singh, A. Singh, S.P. Singh, Effect of citric acid on the hydration of Portland cement, Cem. Concr. Res. 16 (1986) 911–920.

[6] S. Alahrache, F. Winnefeld, J.-B. Champenois, F. Hesselbarth, B. Lothenbach, Chemical activation of hybrid binders based on siliceous fly ash and Portland cement, Cem. Concr. Compos. 66 (2016) 10–23.

[7] J. Stegemann, N. Buenfeld, Neural network modelling of the effects of inorganic impurities on calcium aluminate cement setting, Adv. Cem. Res. 13 (2001) 101–114.

[8] L.E. Burris, K.E. Kurtis, Influence of set retarding admixtures on calcium sulfoaluminate cement hydration and property development, Cem. Concr. Res. 104 (2018) 105–113.

[9] J.E. Barralet, M. Tremayne, K.J. Lilley, U. Gbureck, Modification of calcium phosphate cement with α-hydroxy acids and their salts, Chem. Mater. 17 (2005) 1313–1319.

[10] H. Nguyen, P. Kinnunen, K. Gijbels, V. Carvelli, H. Sreenivasan, A.M. Kantola, V.-V. Telkki, W. Schroeyers, M. Illikainen, Ettringite-based binder from ladle slag and gypsum–the effect of citric acid on fresh and hardened state properties, Cem. Concr. Res. 123 (2019) 105800.

[11] F. Winnefeld, S. Klemm, Influence of Citric Acid on the Hydration Kinetics of Calcium Sulfoaluminate Cement, Submitt. First Int. Conf. Sulphoaluminate Cem. Mater. Eng. Technol, Wuhan China, 2013.

[12] L. Nedyalkova, B. Lothenbach, G. Geng, U. Mäder, J. Tits, Uptake of iodide by calcium aluminate phases (AFm phases), Appl. Geochem. 116 (2020) 104559.

[13] L. Nedyalkova, B. Lothenbach, G. Renaudin, U. Mäder, J. Tits, Effect of redox conditions on the structure and solubility of sulfur-and selenium-AFm phases, Cem. Concr. Res. 123 (2019) 105803.

[14] B. Ma, A. Fernandez-Martinez, S. Grangeon, C. Tournassat, N. Findling, S. Carrero, D. Tisserand, S. Bureau, E. Elkaïm, C. Marini, Selenite uptake by Ca–Al LDH: a description of intercalated anion coordination geometries, Environ. Sci. Technol. 52 (2018) 1624–1632.

[15] B. Ma, A. Fernandez-Martinez, S. Grangeon, C. Tournassat, N. Findling, F. Claret, A. Koishi, N.C. Marty, D. Tisserand, S. Bureau, Evidence of multiple sorption modes in layered double hydroxides using Mo as structural probe, Environ. Sci. Technol. 51 (2017) 5531–5540.

[16] W. Hummel, G. Anderegg, I. Puigdomènech, L. Rao, O. Tochiyama, Chemical Thermodynamics of Compounds and Complexes of U, Np, Pu, Am, Tc, Se, Ni and Zr with selected organic ligands, Elsevier Amsterdam, 2005.

[17] E. Wieland, A. Jakob, J. Tits, B. Lothenbach, D. Kunz, Sorption and diffusion studies with low molecular weight organic compounds in cementitious systems, Appl. Geochem. 67 (2016) 101–117.

[18] L. Van Loon, M. Glaus, S. Stallone, A. Laube, Sorption of isosaccharinic acid, a cellulose degradation product, on cement, Environ. Sci. Technol. 31 (1997) 1243–1245.

[19] M.A. Glaus, A. Laube, L.R. Van Loon, Solid–liquid distribution of selected concrete admixtures in hardened cement pastes, Waste Manag. 26 (2006) 741–751.

[20] I. Androniuk, C. Landesman, P. Henocq, A.G. Kalinichev, Adsorption of gluconate and uranyl on CSH phases: combination of wet chemistry experiments and molecular dynamics simulations for the binary systems, Phys. Chem. Earth Parts A/B/C 99 (2017) 194–203.

[21] Y. Jo, I. Androniuk, N. Çevirim-Papaioannou, B. de Blochouse, M. Altmaier, X. Gaona, Uptake of chloride and iso-saccharinic acid by cement: sorption and molecular dynamics studies on HCP (CEM I) and CSH phases, Cem. Concr. Res. 157 (2022) 106831.

[22] I.G. Richardson, The calcium silicate hydrates, Cem. Concr. Res. 38 (2008) 137–158.

[23] B. Lothenbach, F. Winnefeld, Thermodynamic modelling of the hydration of Portland cement, Cem. Concr. Res. 36 (2006) 209–226.

[24] H.F. Taylor, Cement Chemistry, Thomas Telford London, 1997.

[25] B. Lothenbach, A. Nonat, Calcium silicate hydrates: solid and liquid phase composition, Cem. Concr. Res. 78 (2015) 57–70.

[26] G. Geng, R.J. Myers, M.J.A. Qomi, P.J. Monteiro, Densification of the interlayer spacing governs the nanomechanical properties of calcium-silicate-hydrate, Sci. Rep. 7 (2017) 1–8.

[27] L. Skinner, S. Chae, C. Benmore, H. Wenk, P. Monteiro, Nanostructure of calcium silicate hydrates in cements, Phys. Rev. Lett. 104 (2010) 195502.

[28] J. Li, G. Geng, R. Myers, Y.-S. Yu, D. Shapiro, C. Carraro, R. Maboudian, P. J. Monteiro, The chemistry and structure of calcium (alumino) silicate hydrate: a study by XANES, ptychographic imaging, and wide-and small-angle scattering, Cem. Concr. Res. 115 (2019) 367–378.

[29] N. Krattiger, B. Lothenbach, S.V. Churakov, Sorption and electrokinetic properties of ASR product and CSH: a comparative modelling study, Cem. Concr. Res. 146 (2021) 106491.

[30] T. Matschei, B. Lothenbach, F. Glasser, The AFm phase in Portland cement, Cem. Concr. Res. 37 (2007) 118–130.

[31] D.G. Evans, R.C. Slade, Structural aspects of layered double hydroxides, in: Layered Double Hydroxides, 2006, pp. 1–87.

[32] G. Renaudin, M. Francois, The lamellar double-hydroxide (LDH) compound with composition 3CaO. Al2O3. Ca (NO3) 2.10 H2O, Acta Crystallogr. Sect. C: Cryst. Struct. Commun. 55 (1999) 835–838.

[33] S.M. Leisinger, B. Lothenbach, G. Le Saout, C.A. Johnson, Thermodynamic modeling of solid solutions between monosulfate and monochromate 3CaO• Al2O3• Ca [(CrO4) x (SO4) 1-x]• nH2O, Cem. Concr. Res. 42 (2012) 158–165.

[34] K. Rodgers, S.F. Courtney, New mineral records from Funafuti, Tuvalu: gypsum, brucite, ettringite, Mineral. Mag. 52 (1988) 411–414.

[35] A. Moore, H. Taylor, Crystal structure of ettringite, Nature 218 (1968) 1048–1049.

[36] L. Berry, The unit cell of ettringite, Am. Mineral. J. Earth Planet. Mater. 48 (1963) 939–940.

[37] F. Götz-Neunhoeffer, J. Neubauer, Refined ettringite (Ca6Al2 (SO4) 3 (OH) 12• 26H2O) structure for quantitative X-ray diffraction analysis, Powder Diffract. 21 (2006) 4–11.

[38] R. Snellings, X-ray powder diffraction applied to cement, in: A Practical Guide to Microstructural Analysis of Cementitious Materials 2, 2016, pp. 104–176.

[39] R. Snellings, J. Chwast, Ö. Cizer, N. De Belie, Y. Dhandapani, P. Durdzinski, J. Elsen, J. Haufe, D. Hooton, C. Patapy, Report of TC 238-SCM: hydration stoppage methods for phase assemblage studies of blended cements—results of a round robin test, Mater. Struct. 51 (2018) 1–12.

[40] B.H. O'Connor, M.D. Raven, Application of the Rietveld refinement procedure in assaying powdered mixtures, Powder Diffract. 3 (1988) 2–6.

[41] D. Jansen, F. Goetz-Neunhoeffer, C. Stabler, J. Neubauer, A remastered external standard method applied to the quantification of early OPC hydration, Cem. Concr. Res. 41 (2011) 602–608.

[42] B. Lothenbach, P. Durdzinski, K. De Weerdt, Thermogravimetric analysis, in: A Practical Guide to Microstructural Analysis of Cementitious Materials 1, 2016, pp. 177–211.

[43] L. León-Reina, A. De la Torre, J. Porras-Vázquez, M. Cruz, L. Ordonez, X. Alcobé, F. Gispert-Guirado, A. Larrañaga-Varga, M. Paul, T. Fuellmann, Round robin on Rietveld quantitative phase analysis of Portland cements, J. Appl. Cryst. 42 (2009) 906–916.

[44] P. Stutzman, S. Leigh, Phase analysis of hydraulic cements by X-ray powder diffraction: precision, bias, and qualification, J. ASTM Int. 4 (2007) 1–11.

[45] G. Le Saoût, V. Kocaba, K. Scrivener, Application of the Rietveld method to the analysis of anhydrous cement, Cem. Concr. Res. 41 (2011) 133–148.

[46] E. L'Hôpital, B. Lothenbach, G. Le Saout, D. Kulik, K. Scrivener, Incorporation of aluminium in calcium-silicate-hydrates, Cem. Concr. Res. 75 (2015) 91–103.

[47] C. Jolicoeur, M.-A. Simard, Chemical admixture-cement interactions: phenomenology and physico-chemical concepts, Cem. Concr. Compos. 20 (1998) 87–101.

[48] A. Zingg, F. Winnefeld, L. Holzer, J. Pakusch, S. Becker, L. Gauckler, Adsorption of polyelectrolytes and its influence on the rheology, zeta potential, and microstructure of various cement and hydrate phases, J. Colloid Interface Sci. 323 (2008) 301–312.

[49] M. Kosmulski, Background-subtraction in electroacoustic studies, Colloids Surf. A Physicochem. Eng. Asp. 460 (2014) 104–107.

[50] B. Traynor, H. Uvegi, E. Olivetti, B. Lothenbach, R.J. Myers, Methodology for pH measurement in high alkali cementitious systems, Cem. Concr. Res. 135 (2020) 106122.

[51] T. Wagner, D.A. Kulik, F.F. Hingerl, S.V. Dmytrieva, GEM-Selektor geochemical modeling package: TSolMod library and data interface for multicomponent phase models, Can. Mineral. 50 (2012) 1173–1195.

[52] B. Lothenbach, D.A. Kulik, T. Matschei, M. Balonis, L. Baquerizo, B. Dilnesa, G. D. Miron, R.J. Myers, Cemdata18: a chemical thermodynamic database for hydrated Portland cements and alkali-activated materials, Cem. Concr. Res. 115 (2019) 472–506.

[53] D.A. Kulik, Improving the structural consistency of C-S-H solid solution thermodynamic models, Cem. Concr. Res. 41 (2011) 477–495.

[54] C. De Stefano, A. Gianguzza, D. Piazzese, S. Sammartaus, Speciation of low molecular weight carboxylic ligands in natural fluids: protonation constants and association with major components of seawater of oxydiacetic and citric acids, Anal. Chim. Acta 398 (1999) 103–110.

[55] N. Akram, X. Bourbon, Analyse critique de donnees thermodynamiques: Povoir complexant de l'EDTA, du NTA, du citrate et de l'oxalate vis a vis de cations metalliques, in: ANDRA report C RP O. GES 92, 1996.

[56] P. Blanc, P. Vieillard, H. Gailhanou, S. Gaboreau, N. Marty, F. Claret, B. Madé, E. Giffaut, ThermoChimie database developments in the framework of cement/clay interactions, Appl. Geochem. 55 (2015) 95–107.

[57] H. Sari, Determination of stability constants of citrate complexes with divalent metal ions (M2+ = Mg, Ca, Ni, Cu and Zn) in aqueous solutions solutions, Energy Educ. Sci. Technol. 6 (2001) 85–103.

[58] A. Gácsi, B. Kutus, Á. Buckó, Z. Csendes, G. Peintler, I. Pálinkó, P.M. Sipos, The structure of calcium citrate complex forming in hyperalkaline aqueous solution, J. Mol. Struct. 1118 (2016) 110–116.

[59] D.A. Kulik, T. Wagner, S.V. Dmytrieva, G. Kosakowski, F.F. Hingerl, K. V. Chudnenko, U.R. Berner, GEM-Selektor geochemical modeling package: revised algorithm and GEMS3K numerical kernel for coupled simulation codes, Comput. Geosci. 17 (2013) 1–24.

[60] H.C. Helgeson, D.H. Kirkham, G.C. Flowers, Theoretical prediction of the thermodynamic behavior of aqueous electrolytes by high pressures and

temperatures; IV, calculation of activity coefficients, osmotic coefficients, and apparent molal and standard and relative partial molal properties to 600 degrees C and 5kb, Am. J. Sci. 281 (1981) 1249–1516.
[61] H. Pöllmann, T. Witzke, H. Kohler, Kuzelite,[(SO4)∑ 6H2O], a new mineral from Maroldsweisach/Bavaria, Germany, Neues Jahrbuch f¸ r Mineralogie-Monatshefte, 1997, pp. 423–432.
[62] H.-J. Kuzel, H. Pöllmann, Hydration of C3A in the presence of Ca (OH) 2, CaSO4·2H2O and CaCO3, Cem. Concr. Res. 21 (1991) 885–895.
[63] L.G. Baquerizo, T. Matschei, K.L. Scrivener, M. Saeidpour, A. Thorell, L. Wadsö, Methods to determine hydration states of minerals and cement hydrates, Cem. Concr. Res. 65 (2014) 85–95.
[64] T. Runčevski, R.E. Dinnebier, O.V. Magdysyuk, H. Pöllmann, Crystal structures of calcium hemicarboaluminate and carbonated calcium hemicarboaluminate from synchrotron powder diffraction data, Acta Crystallogr. Sect. B: Struct. Sci. 68 (2012) 493–500.
[65] M. François, G. Renaudin, O. Evrard, A cementitious compound with composition 3CaO. Al2O3. CaCO3. 11H2O, Acta Crystallogr. Sect. C: Cryst. Struct. Commun. 54 (1998) 1214–1217.
[66] H. Pöllman, Minelarogisch-Kristallographische Untersuchugen an Hydratationsprodukten der Aluminatphase hydraulischer Bindemittel (Teil 1), Friedrich-Alexander Universität, Erlagen-Nürnberg, Naturwissenschaftlichen Fakultät, 1989, p. 288.
[67] R. Allmann, Refinement of the hybrid layer structure ($Ca_2Al(OH)_6^+.12SO_4.\ 3H_2O$), in: Neues Jahrbuch für Mineralogie 3, 1977.
[68] F. Von Hoessle, J. Plank, F. Leroux, Intercalation of sulfonated melamine formaldehyde polycondensates into a hydrocalumite LDH structure, J. Phys. Chem. Solid 80 (2015) 112–117.
[69] Q. Wang, C. Taviot-Gueho, F. Leroux, K. Ballerat-Busserolles, C. Bigot, G. Renaudin, Superplasticizer to layered calcium aluminate hydrate interface characterized using model organic molecules, Cem. Concr. Res. 110 (2018) 52–69.
[70] M.U. Okoronkwo, M. Balonis, M. Juenger, M. Bauchy, N. Neithalath, G. Sant, Stability of calcium–alumino layered-double-hydroxide nanocomposites in aqueous electrolytes, Ind. Eng. Chem. Res. 57 (2018) 13417–13426.
[71] J. Zhang, F. Zhang, L. Ren, D.G. Evans, X. Duan, Synthesis of layered double hydroxide anionic clays intercalated by carboxylate anions, Mater. Chem. Phys. 85 (2004) 207–214.
[72] J. Tronto, M.J. dos Reis, F. Silvério, V.R. Balbo, J.M. Marchetti, J.B. Valim, In vitro release of citrate anions intercalated in magnesium aluminium layered double hydroxides, J. Phys. Chem. Solid 65 (2004) 475–480.
[73] C. Geffroy, A. Foissy, J. Persello, B. Cabane, Surface complexation of calcite by carboxylates in water, J. Colloid Interface Sci. 211 (1999) 45–53.
[74] K. Nakamoto, Infrared and Raman Spectra of Inorganic and Coordination Compounds, Part B: Applications in Coordination, Organometallic, and Bioinorganic Chemistry, John Wiley & Sons, 2009.
[75] A. Mesbah, J.P. Rapin, M. François, C. Cau-dit-Coumes, F. Frizon, F. Leroux, G. Renaudin, Crystal structures and phase transition of cementitious Bi-anionic AFm-(Cl−, CO32−) compounds, J. Am. Ceram. Soc. 94 (2011) 261–268.
[76] J. Li, Y. Liu, Y. Gao, L. Zhong, Q. Zou, X. Lai, Preparation and properties of calcium citrate nanosheets for bone graft substitute, Bioengineered 7 (2016) 376–381.
[77] T. Matschei, B. Lothenbach, F.P. Glasser, Thermodynamic properties of Portland cement hydrates in the system CaO–Al2O3–SiO2–CaSO4–CaCO3–H2O, Cem. Concr. Res. 37 (2007) 1379–1410.
[78] B. Lothenbach, T. Matschei, G. Möschner, F.P. Glasser, Thermodynamic modelling of the effect of temperature on the hydration and porosity of Portland cement, Cem. Concr. Res. 38 (2008) 1–18.
[79] S.M. Leisinger, B. Lothenbach, G. Le Saout, R. Kägi, B. Wehrli, C.A. Johnson, Solid solutions between CrO_4- and SO_4-ettringite $Ca_6(Al(OH)_6)_2(Cr_xS_{1-x}O_4)_3$*26 H_2O, Environ. Sci. Technol. 44 (2010) 8983–8988.
[80] M. Zhang, Incorporation of Oxyanionic B, Cr, Mo, and se into Hydrocalumite and Ettringite: Application to Cementitious Systems, University of Waterloo, Waterloo, Canada, 2000, p. 172.
[81] J.-B. Champenois, A. Mesbah, C. Cau Dit Coumes, G. Renaudin, F. Leroux, C. Mercier, B. Revel, D. Damidot, Crystal structures of Boro-AFm and sBoro-AFt phases, Cem. Concr. Res. 42 (2012) (in press).
[82] R.B. Perkins, C.D. Palmer, Solubility of $Ca_6[Al(OH)_6]_2(CrO_4)_3$26$H_2O$, the chromate analogue of ettringite; 5-75°C, Appl. Geochem. 15 (2000) 1203–1218.
[83] I. Baur, C.A. Johnson, The solubility of selenate-AFt (3CaO Al_2O_3 3$CaSeO_4$ 37.5H_2O) and selenate-AFm (3CaO Al_2O_3 $CaSeO_4$ xH_2O), Cem. Concr. Res. 33 (2003) 1741–1748.
[84] S.C. Myneni, S.J. Traina, G.A. Waychunas, T.J. Logan, Vibrational spectroscopy of functional group chemistry and arsenate coordination in ettringite, Geochim. Cosmochim. Acta 62 (1998) 3499–3514.
[85] E. Scholtzová, L. Kucková, J. Kožíšek, D. Tunega, Structural and spectroscopic characterization of ettringite mineral–combined DFT and experimental study, J. Mol. Struct. 1100 (2015) 215–224.
[86] Y. Yan, S.-Y. Yang, G.D. Miron, I.E. Collings, E. L'Hôpital, J. Skibsted, F. Winnefeld, K. Scrivener, B. Lothenbach, Effect of alkali hydroxide on calcium silicate hydrate (CSH), Cem. Concr. Res. 151 (2022) 106636.
[87] S. Grangeon, F. Claret, Y. Linard, C. Chiaberge, X-ray diffraction: a powerful tool to probe and understand the structure of nanocrystalline calcium silicate hydrates, Acta Crystallogr. Sect. B: Struct. Sci. Cryst. Eng. Mater. 69 (2013) 465–473.
[88] S. Masoumi, S. Zare, H. Valipour, M.J. Abdolhosseini Qomi, Effective interactions between calcium-silicate-hydrate nanolayers, J. Phys. Chem. C 123 (2019) 4755–4766.
[89] N.V. Chukanov, IR Spectra of Minerals and Reference Samples Data, Springer, Infrared spectra of mineral species, 2014, pp. 21–1701.
[90] P. Yu, R.J. Kirkpatrick, B. Poe, P.F. McMillan, X. Cong, Structure of calcium silicate hydrate (C-S-H): near-, mid-, and far-infrared spectroscopy, J. Am. Ceram. Soc. 82 (1999) 742–748.
[91] A. Vidmer, G. Sclauzero, A. Pasquarello, Infrared spectra of jennite and tobermorite from first-principles, Cem. Concr. Res. 60 (2014) 11–23.
[92] K. Mesecke, L.N. Warr, W. Malorny, Structure modeling and quantitative X-ray diffraction of C-(a)-SH, J. Appl. Cryst. 55 (2022).
[93] L. Nedyalkova, J. Tits, G. Renaudin, E. Wieland, U. Mäder, B. Lothenbach, Mechanisms and thermodynamic modelling of iodide sorption on AFm phases, J. Colloid Interface Sci. 608 (2022) 683–691.
[94] L. Aimoz, E. Wieland, C. Taviot-Guého, R. Dähn, M. Vespa, S.V. Churakov, Structural insight into iodide uptake by AFm phases, Environ. Sci. Technol. 46 (2012) 3874–3881.
[95] L. Bouzouaid, B. Lothenbach, A. Fernandez-Martinez, C. Labbez, Gluconate and hexitols effects on CSH solubility, Cem. Concr. Res. 160 (2022) 106894.
[96] M. Turesson, C. Labbez, A. Nonat, Calcium mediated polyelectrolyte adsorption on like-charged surfaces, Langmuir 27 (2011) 13572–13581.
[97] L. Nachbaur, P.-C. Nkinamubanzi, A. Nonat, J.-C. Mutin, Electrokinetic properties which control the coagulation of silicate cement suspensions during early age hydration, J. Colloid Interface Sci. 202 (1998) 261–268.
[98] H. Viallis-Terrisse, A. Nonat, J.C. Petit, Zeta-potential study of calcium silicate hydrates interacting with alkaline cations, J. Colloid Interface Sci. 253 (2001) 140–149.
[99] R. Barbarulo, H. Peycelon, S. Prene, Experimental study and modelling of sulfate sorption on calcium silicate hydrates, Ann. Chim.: Sci. des Materiaux (Paris) 28 (2003) S5–S10.
[100] L. Ferrari, J. Kaufmann, F. Winnefeld, J. Plank, Interaction of cement model systems with superplasticizers investigated by atomic force microscopy, zeta potential, and adsorption measurements, J. Colloid Interface Sci. 347 (2010) 15–24.
[101] C. Labbez, I. Pochard, B. Jönsson, A. Nonat, CSH/solution interface: experimental and Monte Carlo studies, Cem. Concr. Res. 41 (2011) 161–168.
[102] S.V. Churakov, C. Labbez, L. Pegado, M. Sulpizi, Intrinsic acidity of surface sites in calcium silicate hydrates and its implication to their electrokinetic properties, J. Phys. Chem. C 118 (2014) 11752–11762.
[103] J. Haas, A. Nonat, From C–S–H to C–A–S–H: Experimental study and thermodynamic modelling, Cem. Concr. Res. 68 (2015) 124–138.
[104] S. Barzgar, B. Lothenbach, M. Tarik, A. Di Giacomo, C. Ludwig, The effect of sodium hydroxide on Al uptake by calcium silicate hydrates (CSH), J. Colloid Interface Sci. 572 (2020) 246–256.
[105] G. Wynn-Jones, R.M. Shelton, M.P. Hofmann, Injectable citrate-modified Portland cement for use in vertebroplasty, J. Biomed. Mater. Res. Part B Appl. Biomater. 102 (2014) 1799–1808.
[106] F. Deschner, F. Winnefeld, B. Lothenbach, S. Seufert, P. Schwesig, S. Dittrich, F. Goetz-Neunhoeffer, J. Neubauer, Hydration of Portland cement with high replacement by siliceous fly ash, Cem. Concr. Res. 42 (2012) 1389–1400.
[107] B. Lothenbach, K. Scrivener, R. Hooton, Supplementary cementitious materials, Cem. Concr. Res. 41 (2011) 1244–1256.
[108] I.R. de Oliveira, A.R. Studart, F.A.O. Valenzuela, V.C. Pandolfelli, Setting behavior of ultra-low cement refractory castables in the presence of citrate and polymethacrylate salts, J. Eur. Ceram. Soc. 23 (2003) 2225–2235.